

# Experimental and numerical FEM of woven GFRP composites during drilling

Mohamed S. Abd-Elwahed<sup>1</sup>, Usama A. Khashaba<sup>1,2</sup>, Khaled I. Ahmed<sup>1</sup>, Mohamed A. Eltaher<sup>\*1,2</sup>,  
Ismael Najjar<sup>1</sup>, Ammar Melaibari<sup>1</sup> and Azza M. Abdraboh<sup>3</sup>

<sup>1</sup>Mechanical Engineering Department, Faculty of Engineering, King Abdulaziz University, P.O. Box 80204, Jeddah 22254-2265, Saudi Arabia

<sup>2</sup>Mechanical Design and Production Engineering Department, Faculty of Engineering, Zagazig University, Egypt

<sup>3</sup>Physics Department, Faculty of Science, Banha University, Banha, Egypt

(Received May 31, 2021, Revised September 19, 2021, Accepted September 24, 2021)

**Abstract.** This paper investigates experimentally and numerically the influence of drilling process on the mechanical and thermomechanical behaviors of woven glass fiber reinforced polymer (GFRP) composite plate. Through the experimental analysis, a CNC machine with cemented carbide drill (point angles  $\phi=118^\circ$  and 6 mm diameter) was used to drill a woven GFRP laminated squared plate with a length of 36.6 mm and different thicknesses. A produced temperature during drilling “heat affected zone (HAZ)” was measured by two different procedures using thermal IR camera and thermocouples. A thrust force and cutting torque were measured by a Kistler 9272 dynamometer. The delamination factors were evaluated by the image processing technique. Finite element model (FEM) has been developed by using LS-Dyna to simulate the drilling processing and validate the thrust force and torque with those obtained by experimental technique. It is found that, the present finite element model has the capability to predict the force and torque efficiently at various drilling conditions. Numerical parametric analysis is presented to illustrate the influences of the speeding up, coefficient of friction, element type, and mass scaling effects on the calculated thrust force, torque and calculation’s cost. It is found that, the cutting time can be adjusted by drilling parameters (feed, speed, and specimen thickness) to control the induced temperature and thus, the force, torque and delamination factor in drilling GFRP composites. The delamination of woven GFRP is accompanied with edge chipping, spalling, and uncut fibers.

**Keywords:** drilling of composite; finite element analysis; mass scaling and speeding up; thrust force and torque; woven glass fiber

## 1. Introduction

Fiber reinforced polymer (FRP) composite laminates possess attractive characteristics such as chemical resistance, low weight, design flexibility, high strength and high stiffness-to-weight ratio. These properties account for manufacturing of structural parts with FRP composite in the aircraft and spacecraft industries, railway, automobile, aeronautical, marine vehicles, pressure vessels, and sporting goods, wind energy, mechanical and plant engineering, (Khashaba and Ramzi 2017, Reisgen *et al.* 2020). For instance, about 57% of the primary structure of Boeing 787 (Dream-liner) consists of composites, which can save 15-20% fuel for a comparable mission compared to any other wide body airplane, Geng *et al.* (2019). Laminated composite structures are made-up of composite materials plies with desirable angle orientations to accomplish desirable and high-performance mechanical properties, Eltaher and Mohamed (2020). Machining operation, such as drilling of FRP laminates, plays a significant role in the assembly of parts in aircraft and spacecraft production. conventional drilling with twist or special drill bits has remained the most frequently and economically used machining operation in industry, Karimi *et al.* (2016). Due

to its heterogeneity and anisotropy, FRP laminates becomes one of the typical difficult-to machining materials, Shabri *et al.* (2020). A drilling process of composite is a common machining operation, which is still an open problem for the academic and industry. The quality of the drilled holes such as roughness/waviness of its wall surface, roundness, and axial straightness of the hole section causes high stress on the rivet, leading to its failure. Microcracking and delamination owing to drilling process significantly reduces the composites residual strength. Therefore, the quality of the drilled holes can be critical to the life of the riveted joints for which the holes are used, Khashaba (2013).

In 1990, Ho-Cheng *et al.* and Tagliaferri *et al.* investigated and predicted the damage zone and delamination of laminated composite induced during drilling by using a fracture mechanics approach. Khashaba *et al.* (2007) examined the influence of drilling parameters on cutting forces and torques in drilling chopped composites and predicted that delamination size decreased with decreasing the feed and insignificant affect by cutting speed. Shyha *et al.* (2009) evaluated the effect of drill geometry and drilling conditions on tool life and hole quality of unbacked carbon CFRP laminate. Khashaba *et al.* (2010) showed that the behavior of thrust force during drilling process was greatly affected by the drill pre-wear, and peaks/valleys in surface roughness profile were due to burning the matrix. Durão *et al.* (2010) monitored hole wall roughness and delamination during drilling of composite

\*Corresponding author, Professor  
E-mail: meltaher@kau.edu.sa

laminates by different drill point geometries and feed rates. Gaitonde *et al.* (2011) indicated that point angle is the most significant factor followed by feed and spindle speed on delamination defects. Kharazan *et al.* (2014) investigated delamination growth in composite laminates subjected to low-velocity impact. Mahieddine *et al.* (2015) presented modeling and simulation of partially delaminated composite beams by using first-order shear deformation theory. Luo *et al.* (2016) observed in drilling thin CRFP laminates that when uncut thickness was too thin to hold the drill bit, spring back of workpiece enlarged the actual feed rate. Merino-Pérez *et al.* (2016) studied impact of cutting speed and workpiece constituents on the forces developed in CFRP drilling by machining three carbon/epoxy systems, combining two types of thermosetting resins and two types of woven CF fabrics. Biswal *et al.* (2016) experimentally studied the critical loads of laminated composite cylindrical shell panels that are made of hygrothermal treated woven fiber-glass/epoxy by using a universal testing machine INSTRON 8862, Khashaba and El-Keran (2017) investigated experimentally and analytically the impact of machining parameters on thrust force and delamination during a drilling of thin woven GFRP. Qiu *et al.* (2018) considered effects of chisel edge and step drill on delamination of CFRP during drilling and demonstrated that the chisel edge has significant influence on delamination when the different ratio of primary drill bit diameter to secondary drill bit diameter ( $k$ ) is bigger than 0.75. Fazilati (2018) investigated the parametric instability characteristics of tow-steered variable stiffness composite laminated cylindrical panels using the B-spline finite strip method considering geometrical defects including cutout and delamination. Ghosh and Chakravorty (2019) used the finite element method to predict failure on the first ply of composite hyper shells with various edge conditions. Geier *et al.* (2019) developed a comprehensive review on advanced cutting tools and technologies for drilling carbon fiber reinforced polymer (CFRP) composites.

In the work conducted by Cadorin *et al.* (2015), it was found the reinforcement of the composite material in the third direction remove the problem of delamination at the hole exit even the tool is worn and for high feed rate used. Beylergil *et al.* (2019) showed that the propagation Mode-I fracture toughness values of carbon fiber/epoxy (CF/EP) composites can be significantly improved (by about 72%) using aramid nonwoven fabrics. Formisano *et al.* (2020) evaluated the influence of the manufacturing technology on the mechanical behavior of composite laminates from commingled fabrics consisting of glass and polypropylene fibers. Gemi *et al.* (2020) studied damage and surface quality of filament wound hybrid composite pipes with different stacking sequences during drilling. Khashaba *et al.* (2020) explored experimentally thrust force, torque and delamination of GFRP composites during drilling processes with different machining parameters. Mudhukrishnan *et al.* (2020) analyzed the thrust force and delamination in drilling of GFR polypropylene composites using HSS twist, tipped carbide and solid carbide drills, and observed that higher value of thrust force is noticed with HSS rather than the other types. Suresh *et al.* (2020)

restored the strength of the repaired sandwich beams after complete failure by insertion of submillimeter fibrous pins in the failed laminate and the honeycomb cells using robotic hand micro-drilling. Zou *et al.* (2020) addressed cutting responses of the hole characteristics and tool wear modes during drilling process of carbon fiber-reinforced plastic/Al co-cured material with standard TiAlN-coated cemented carbide twist drill. Mishra *et al.* (2020) developed a numerical simulation model to present the influence of residual thermal stresses and material anisotropy on the inter-laminar delamination behavior of the joint structure. Ahmadi and Zeinedini (2020) investigated effect of drilling on the mode I delamination of GFRP laminates by using experimental, theoretical, and numerical methods. Eltahir and Abdelrahmaan (2020), Almitani (2020) studied the bending and buckling of perforated nanobeam with surface energy effects. Jai *et al.* (2020a) presented novel multi-margin drill structure for improving drilling quality/accuracy of Ti/CFRP stack.

Considering thermal effects, Ramesh *et al.* (2016) presented the influence of different cooling methods on quality characteristics of drilled GFRP non-laminated 20 mm thick pultruded composite rods. In the work conducted by Zitoune *et al.* (2017) an original technique for the measurement of the machining temperature has been proposed. This technique is based on the in-situ instrumentation with optical fiber with Bragg sensors for the monitoring when in real time of the temperature generated when drilling thick 3D woven composites. It was concluded that, the temperature generated when drilling is conducted with twist drill coated with TiN/AlTiN/CrAlSiN is inferior the one generated when drilling with the same drill coated with TiN/TiAlSiN/AlTiSiN. This result has been attributed to the frictional phenomenon between the tool and the CFRP. Hou *et al.* (2020) investigated impacts of drilling parameters involving rotating speed, feed rate and diameter of twist drill on exit-ply temperature characteristics and damages of UD CFRP. Zhang *et al.* (2020, 2021) analyzed influences of the axial force and the hole-exit temperature on the formation of the hole-exit surface damages and predicted novel fiber fracture criteria in machining process of CFRP.

Through analytical and numerical analysis, Karimi *et al.* (2016) modeled the critical feed rate for the onset of delamination by combining the resulting equations for oblique cutting model and critical thrust force based on elastic fracture mechanics (EFM) and classical plate bending theory (CPBT). Elamary *et al.* (2016) presented a numerical simulation of concrete beams reinforced with composite GFRP-Steel bars under three points bending. Ismail *et al.* (2017), Ojo *et al.* (2017) developed an analytical model using linear elastic fracture mechanics and CPBT to evaluate the delamination of FRP during drilling operation, and predicted that thrust force, feed rate, twist drill bit chisel edge and point angle are the principal factors responsible for delamination. Tan and Azmi (2017) presented analytical mechanics formulation with surface energy released from the crack surface to predict critical thrust force for on-set delamination damage of drilling hybrid FRP composite. Shetty *et al.* (2017) presented a brief

review in depth for drilling of composites using finite element method and knowledge on damage of the composites caused during drilling. Joshi *et al.* (2018) developed FEM for the study of delamination while drilling FRP composites. The simulations use realistic geometry and boundary conditions, and the results are compared with literature, analytical models, and experimental results. Hrechuk *et al.* (2018) exploited non-destructive quantification of visible defects based on the numerical analysis to evaluate the quality of drilled holes in FRP composites. Guenfoud *et al.* (2018) used of the strain approach to develop a new consistent triangular thin flat shell finite element with drilling rotation. Based on the microscopic level, Tang *et al.* (2018) developed 3D finite element model to examine the chip formation and delamination in drilling of CFRP composites. Murthy *et al.* (2019) used a system dynamic approach and Taguchi method to evaluate the influence of drilling parameters on thrust force developed during drilling of GFRP. Feito *et al.* (2019) predicted the damage induced during drilling of composite materials by using multi-objective optimization analysis of cutting parameters for special geometry drills. Heidary *et al.* (2020) estimated the critical thrust force and feed rate determination in drilling of GFRP laminate with backup plate. Liu *et al.* (2020a, b) presented delamination model based on superposition of linear fracture mechanics capable of predicting a critical thrust force of aramid fiber-reinforced plastics by brad drill. Wang and Jia (2020) performed a full factorial experiment and Artificial neural network for the drilling of CFRP with different drilling parameters to express thrust force and delamination factor as a function of drilling parameters. Shahri *et al.* (2020) exploited modified Mindlin-Reissner plate theory in conjunction with EFM in mixed mode loading condition for the prediction of critical thrust force during drilling process. Tong *et al.* (2020) developed experimental and analytical study on continuous GFRP concrete decks with steel bars. Jai *et al.* (2020b) presented analytical study of delamination damage and delamination-free drilling method of CFRP composite. Asiri *et al.* (2020), Eltaher and Akbas (2020) developed a finite element model to predict the transient response of 2D functionally graded beam under a dynamic load. She (2020), She *et al.* (2021), Lu *et al.* (2021) studied numerically resonance analysis and postbuckling of composite curved microbeams reinforced with graphene nanoplatelets. Zhang *et al.* (2021) investigated the snap-buckling of FGCNTR curved nanobeams considering surface effects. She (2021) presented the effect of thermal loadings on guided wave propagation of porous functionally graded plates. Bhat *et al.* (2020) investigated the effect of operational parameters on the damages caused in the GFRP composites during the drilling process by using multiple response optimization technique. In another work Saoudi *et al.* (2016) proposed an analytical model to predict the critical thrust force responsible for delamination at the hole exit. Almitani *et al.* (2021) exploited finite element model to evaluated stress and vibration analysis of axially functionally graded rotating beams.

According to the knowledge of author and literature review, the impact of thermomechanical behavior of the woven GFRP plate under drilling using experimental and

Table 1 The estimated fiber volume fraction

$n$ (Layers)	$A_w$ (g/m <sup>2</sup> )	$\rho_f$ (g/cm <sup>3</sup> )	$t$ (cm)	$V_f$ (%)
8	324	2.5	0.259	40.0
16	324	2.5	0.525	39.5
24	324	2.5	0.773	40.2

numerical finite element model (FEM) has not been addressed. Therefore, the current article aims to fill this gap. The investigation of the temperature induced by drilling has been considered by a thermocouple and thermal imaging infrared camera. The impact of machining parameters (i.e., speed, feed, etc.) and numerical parameters (i.e., model speeding up, Mass scaling, Element Type, Coefficient of friction, and strain rate) on the thrust force, torque and delamination has been evaluated. The rest of the paper is organized as following, the experimental setup and material characterization have been presented in section 2. The experimental results are discussed comprehensively in section 3. The numerical model and adaptation have been discussed in section 4. Validation of the numerical model with experimental thrust force and torque is presented in section 5, with parametric studies. Statistical analysis is illustrated in section 6. The conclusion remarks and main points are summarized in section 7.

## 2. Experimental works

### 2.1 Specimen preparation

Three woven GFRP composite laminates with varying thickness were manufactured using hand lay-up technique. The polymer (epoxy) matrix was Araldite LY5138-2 and Hardener HY5138. Symmetric lay-ups of orthogonal balanced woven fabric composites with thickness of 2.6, 5.3 and 7.7 mm were manufactured respectively from 8, 16 and 24 layers of E-woven roving glass-fiber (3.5 yarns/cm for the warp and weft fibers). The cutting of glass fiber layers was through the warp and weft threads to ensure right angles of all layers. The fiber volume fractions of the fabricated GFRP laminates were calculated by Eq. (1) and presented in Table 1.

$$V_f = \frac{n * A_w}{\rho_f * t} \quad (1)$$

where  $V_f$  is the fiber volume fraction,  $n$  is the number of layers,  $A_w$  is the areal weight of the fabric,  $t$  is the thickness of the product, and  $\rho_f$  the fiber density.

### 2.2 Macromechanical characterization

According to ASTM D 3039, a series of standard ASTM tensile tests were performed to characterize the mechanical properties of the fabricated materials using Servohydraulic testing machine model Instron 8803 (500 kN) and 8872 (10 kN). The test specimens were cut to the standard dimension using CNC abrasive waterjet machine to eliminate a heat that generated by conventional machining processes. The specimens were loaded at test rate of 1.0 mm/min. The

Table 2 The mechanical properties of woven GFRP composites

Poisson's ratio $\nu_{12}=\nu_{21}$	Standard Deviation	Young's modulus (GPa) $E_{11}=E_{22}$	Standard Deviation	Tensile Strength (MPa)	Standard Deviation
0.295	0.015	16.05	0.116	203.86	4.215

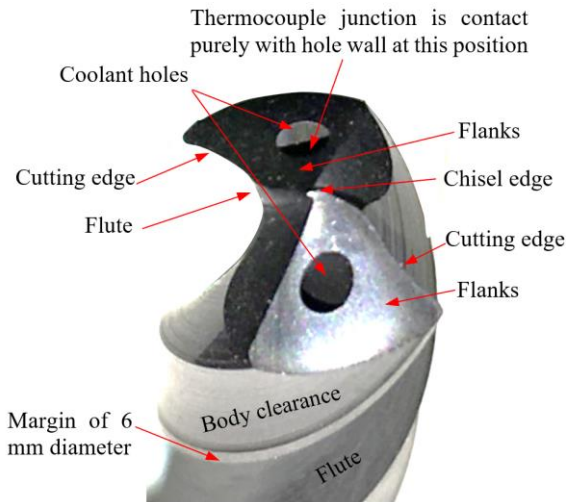


Fig. 1 Different elements of the cemented carbide drill

longitudinal and transverse strains were measured using 4-channels data acquisition (DAQ) model 9237 NI. For each test, five samples were evaluated, and the average value was presented in Table 2.

### 2.3 Drilling experimental setup

Drilling tests were conducted under dry cutting conditions using CNC milling machine model "Deckel Maho DMG DMC 1035 V, ecoline". Two flute-twist drills manufactured from special ultra-fine cemented carbide particle, are used for efficient cutting, with excellent toughness and abrasion resistance. As provided by the manufacturer (Zhuzhou Best for Tools Co., Ltd., China), the details about drill materials were illustrated in Table 3 and the drills geometries are illustrated in Table 4. The drills were provided with two internal coolant holes of 0.6 mm diameter. Three identical drills were used in this study. The total cutting time for each drill does not exceed 4 min, which is too small to induce wear in the cemented carbide drill. The different elements of the drill, which are repeated in the result and discussion section are illustrated in Fig. 1.

The drilling tests were implemented on specimens of

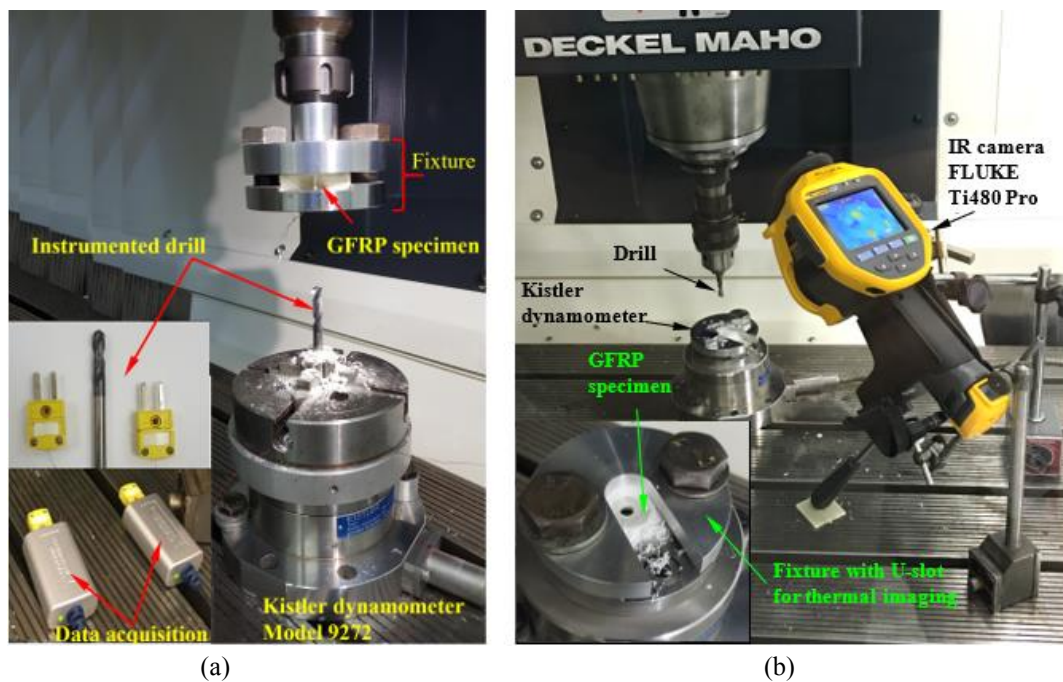


Fig. 2 Experimental setup for measuring cutting forces in drilling GFRP composites using CNC milling machine and Kistler dynamometer. The temperature was measured by: (a) instrumented drill with two thermocouples, and (b) IR camera

Table 3 The constituent materials of the cemented carbide drills

Material grade	ISO code	WC	Co	Grain size ( $\mu\text{m}$ )	Density ( $\text{g}/\text{cm}^3$ )	Hardness (HRA)	Transverse rupture strength (MPa)	$K_{IC}$ ( $\text{MPa}\cdot\text{m}^{1/2}$ )
K200	K20-K40	90%	10%	0.5-0.8	14.4	91.3	3920	10.5

Table 4 Geometries of the cemented carbide drills, as provided by the manufacturer

D (mm)	Flute length (mm)	Overall length (mm)	Helix angle	Rake angle	Clearance angle	Point angle	Chisel edge length (mm)
6	28	66	30°	30°	12°	118°	0.3

Table 5 Levels of the variables used in the experiment

Factors	Unit	Levels			
		1	2	3	4
Spindle speed, $N$	r/min	400	800	1600	--
Feed, $f$	mm/r	0.025	0.05	0.1	0.2
Thickness of sample, $t$	mm	2.6	5.3	7.7	--

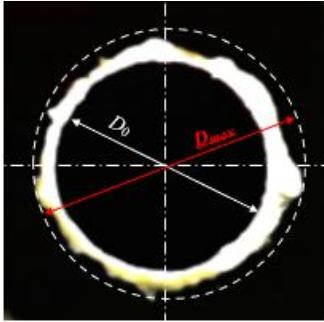


Fig. 3 Image indicates the push-out delamination in drilling FRP composites

36.6×36.6 mm prepared from composite laminates using abrasive water jet machine. The experimental setup with dynamometer–fixture–workpiece assembly is illustrated in Fig. 2. Thrust force and torque data were recorded with a Kistler 9272. For the drilling parameters a full experimental design is used through spindle speed ( $N$ ), feed ( $f$ ), and laminate thickness ( $t$ ) as illustrated in Table 5. Three tests were performed for each machining factor.

The temperature was measured using two different techniques. In the first technique, two K-thermocouples model TL0201 were embedded in coolant holes near the cutting edge of the drill. The temperature variation during the drilling process was online monitored and recorded using National Instruments LabVIEW Signal Express software. In this method, the instrumented drill was mounted by four independent-jaws chuck, which was fixed on the dynamometer. The specimen was clamped firmly to the machine spindle using special fixture as shown in Fig. 2(a). In the second technique, the specimen was clamped firmly on the dynamometer using special fixture as shown in Fig. 2(b). The fixture was designed with U-slot of 20 mm width to allows measuring the temperature induced in the heated zone using infrared (IR) camera model FLUKE Ti480 Pro, which has 640×480 resolution and temperature measurement range from  $\leq -20^{\circ}\text{C}$  to  $+800^{\circ}\text{C}$ . The infrared camera placed at about 260 mm from the hole center and at angle of  $60^{\circ}$  as shown in Fig. 2(b). The recorded video for each test were analyzed using SmartView 4.3 software.

#### 2.4 Delamination characterization

The peel-up and push-out surface delaminations had been measured using the AutoCAD technique that was developed earlier by Khashaba (2004). This technique is suitable for quasi-transparent composite materials in which the drilled specimen was scanned using high resolution flatbed color scanner model Epson “V370, 4800×9600 dpi”. The transmitted light to the delaminated or damaged zone

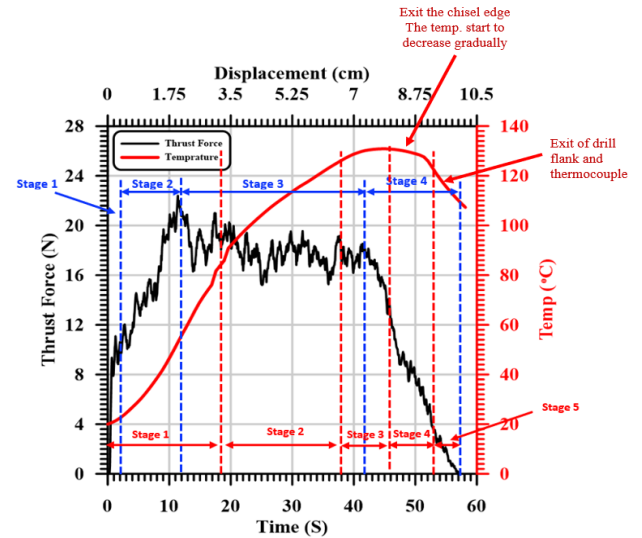


Fig. 4 Evolution of thrust force and the induced temperature vs time (displacement) in drilling GFRP with 7.7 mm thickness at 400 r/min and 0.025 mm/r

makes it brighter and can be easily distinguished from the undamaged area. The image was analyzed using CorelDraw software, which enable magnifying the image and determine the delamination size within  $10^{-3}$  mm. The delamination factor was defined as

$$F_d = \frac{D_{\max}}{D_0} \quad (2)$$

in which  $F_d$  is the delamination factor,  $D_{\max}$  is the maximum delaminated diameter that drawn from the centerline of the hole nominal diameter ( $D_0=6$  mm), Fig. 3.

### 3. Experimental discussion

#### 3.1 Thrust force and temperature relationship

Fig. 4 illustrates the evolution of the thrust force and temperature with respect to cutting time and displacement during drilling of woven GFRP composite with thickness of 7.7 mm at 400 r/min cutting speed and 0.025 mm/r feed. As shown, the thrust force and temperature vs time can be categorized to four and five different stages, respectively, as follows:

In the 1<sup>st</sup> stage the GFRP composite behaves in a linear elastic manner up to thrust force of about 12 N (around 52% of the maximum  $F_t$ ) within 2 sec ( $2 \times 400 \times 0.025 / 60 = 0.33$  mm) at the entry of chisel edge into the workpiece. At this stage the chisel edge, with zero speed at its center, does not actually cut, but, instead, it extrudes the material. Chandrasekharan *et al.* (1995), Khashaba *et al.* (2007) reported that the average chiseling edge thrust force is about 53% of the total thrust force.

At the end of the 1<sup>st</sup> stage, the drill penetrates the workpiece surface layer, and second the 2<sup>nd</sup> stage was observed. In this stage the thrust force increased from 12 N to its maximum value of 23 N as drill moves to 1.8 mm. This distance equal the approach allowance that accounts

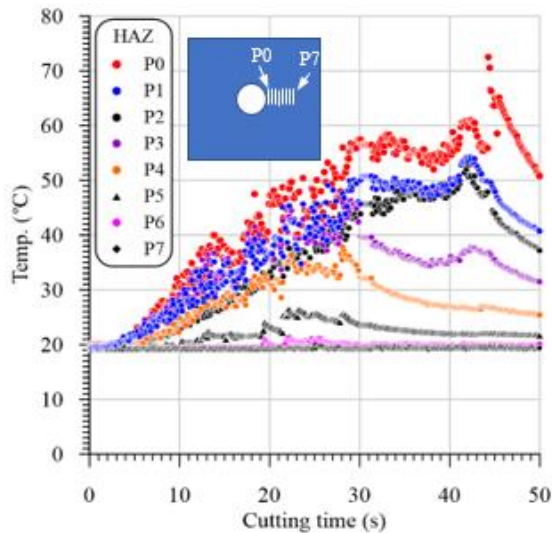


Fig. 5 Representative sample of evolution of temperature obtained by IR camera vs cutting time in drilling GFRP with 5.3 mm thickness at 400 r/min and 0.025 mm/r at different positions

for the drill point angle of  $118^\circ$ ,  $=(D/2)/\tan(118/2)=1.8$  mm. During this stage, the uncut chip area increases with the increase of the cutting depth until the total engagement of the drill point was achieved. After this distance, the drill is fully engaged with work piece and the 3<sup>rd</sup> stage will be initiated. During the 1<sup>st</sup> and 2<sup>nd</sup>, the flank temperature was increased sharply because of rapidly increase in the tool-workpiece contact/cutting area.

In 3<sup>rd</sup> stages, the temperature was increased with increasing hole depth because of increasing of friction between drill margin and the machined surface. The accumulated temperature in the 3<sup>rd</sup> stage was increased with a lower rate (slope) compared to those of the 1<sup>st</sup> and 2<sup>nd</sup>. The increase of the accumulated drill temperature was assisted by the lower thermal conductivity of the GFRP composites. Khashaba *et al.* (2010) showed that the thermal conductivity of GFRP composites is very low ( $0.59$  W/m $^\circ$ C) compared to steel ( $=53$  W/m $^\circ$ C), brass ( $=109$  W/m $^\circ$ C) and Aluminum ( $=210$  W/m $^\circ$ C). The thermal conductivity of glass fiber is ( $8.67$  W/m $^\circ$ C) higher than that of the epoxy resin ( $0.14$  W/m $^\circ$ C). Therefore, the heat accumulation during cutting mostly occurs in the resin matrix. In addition, the glass fiber has a much higher glass transition temperature ( $T_g=550^\circ$ C) compared to the epoxy matrix. The  $T_g$  of used epoxy is ( $60.61^\circ$ C) determined in the present work by Differential Scanning Calorimetry (DSC). The lower thermal conductivity and  $T_g$  of epoxy matrix played a vital role on its softening and burning and thus, the measured machineability parameters such as thrust force, torque and delamination factor as will be seen later.

For the third stage, thrust force is decreased gradually, which may be attributed to a reduction in stiffness of the specimen that is caused by the removal of material layers under the drill as well as softening of the material due to increasing of cutting temperature. Through this stage, the temperature increased linearly until 6.7 mm after 38 s. At this point equilibrium balance between the energy generated

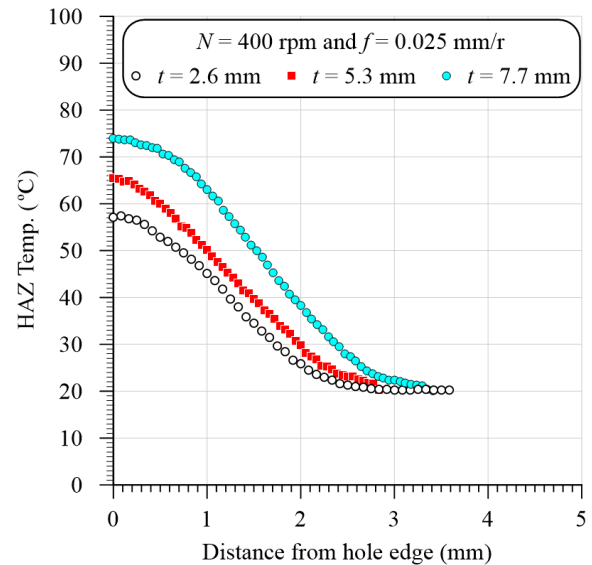


Fig. 6 Representative sample of the temperature distribution of HAZ of GFRP specimen with different thicknesses at 400 r/min and 0.025 mm/r

by friction and energy stored in drill and workpiece. Therefore, the temperature remain constant as the drill moves from 6.7 mm to 8.3 mm (the third stage of temperature).

The fourth stage start when the chisel edge of the drill just exits the specimen causing a higher reduction in thrust force by about 50%. Then gradual reduction in the thrust force and temperature fifth stage are observed up to the end of the drilling cycle due to the gradual exit of the drill cutting edges, as shown in Fig. 4.

### 3.2 Machining variables vs temperature

Fig. 5 shows a representative sample of evolution of the measured temperature using the IR camera versus cutting time in drilling GFRP with 5.3 mm thickness at 400 r/min and 0.025 mm/r at different positions. To obtain the heat distribution in the heat affected zone (HAZ), a line of about 5mm is drawn from the hole edge at the middle of the U-slot using the utilities of SmartView 4.3 software. A large number of temperature measurements along the drawn line were obtained and recorded, as illustrated in Fig. 6. This figure shows representative samples of the temperature distribution in the HAZ of the GFRP composites with different thickness at speed of 400 rpm and feed of 0.025 mm/r. The results in Fig. 6 showed that the temperature of the HAZ was sharply decreased as move away from the hole edge because of the lower thermal conductivity of the GFRP composite laminates. The temperature was reached to the room temperature of about  $20^\circ$ C after about 2.8 mm, 3 mm and 3.4 mm away from the hole edge of the composite laminates with thickness of 2.6 mm, 3.5 mm and 7.7 mm, respectively. Merino-Pérez *et al.* (2015) found that the temperature was decreased from  $360^\circ$ C to  $50^\circ$ C after 3.5 mm from the hole edge in drilling FRP composites at speed ranging from 50 to 200 m/min. They have measured the temperature distribution using thermal imaging and

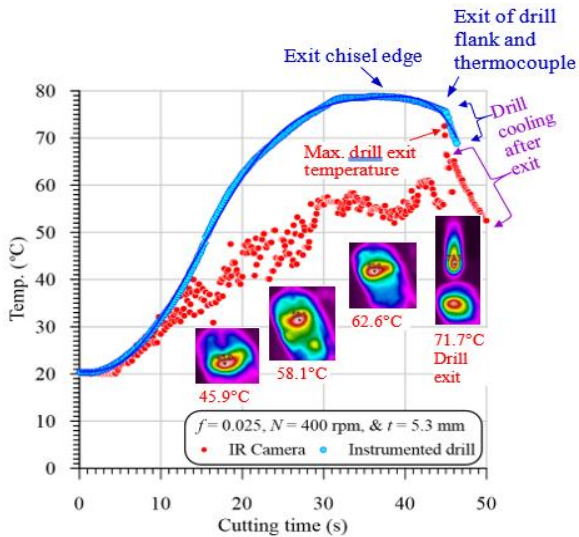
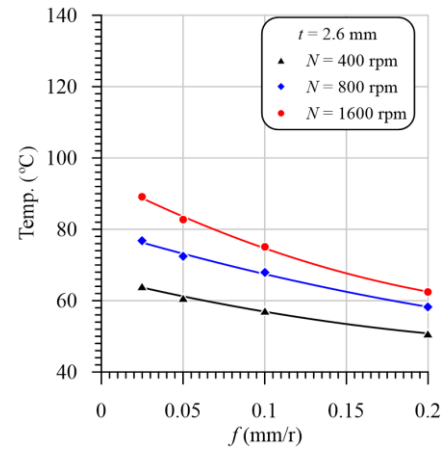


Fig. 7 Representative sample of evolution of temperature at hole edge (PO) vs cutting time in drilling GFRP with 5.3 mm thickness at 400 r/min and 0.025 mm/r

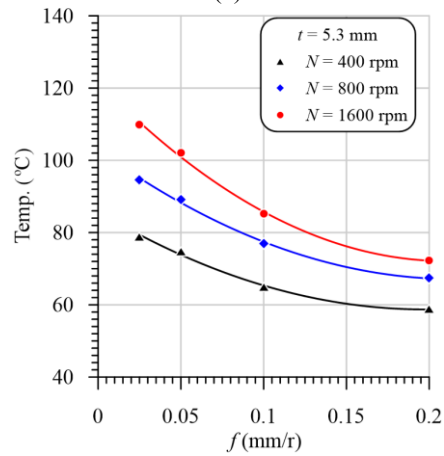
thermocouples impeded at different distances around the hole.

Fig. 7 illustrates a representative sample of evolution of temperature vs cutting time in drilling GFRP with 5.3 mm thickness at 400 r/min and 0.025 mm/r. The temperature was measured by both the instrumented drill and the IR-camera. It is clear from Fig. 7 that at the first 10 s the measured temperature values by the two methods are almost identical. This was attributed to at the drill entry, the chisel edge with zero speed at its center does not actually cut, but instead, it extrudes the material. Therefore, the camera records the drill temperature that equal to those measured using the instrumented drill. Similar observation was reported by Xu *et al.* (2020) in drilling CFRP/Ti6Al4V stacks. After 10-s the drill point is cut only 1.67 mm ( $10 \times f \times N / 60$ ) from its approach allowance (1.8 mm). Therefore, the camera measure in the first 10-s the temperature of drill pint, which approximately equal those measured by the instrumented drill. As the drill penetrate the specimen, the drill-work interaction zone become not accessible and thus, the IR camera measure the temperature of the HFZ, which is lower than that of the drill point that was measured by the instrumented drill, as shown in Fig. 7. At drill exit the work, the IR camera record sudden increase of the temperature. This because the camera always records the highest temperature in the drilling zone. This result indicates that the drill point temperature (72°C) is higher than those of the hole edge (62°C) by about 10°C, as shown in Fig. 7.

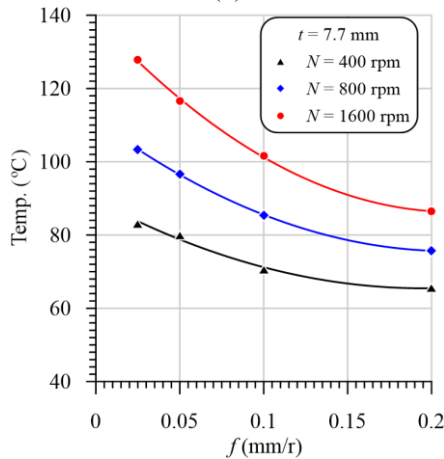
Fig. 8(a)-(c) shows the variation of drill temperature vs feed with varying cutting speeds in drilling GFRP composites with thickness of 2,6, 5.3 and 7.7 mm, respectively. It is evident from these figures that for the investigated cutting speeds and laminate thicknesses, the peak flank temperature is proportional inversely with the feed because of decreasing cutting time. In contrast, at the same feed values, the maximum temperature curves were observed at maximum speed and laminate thickness, as



(a)



(b)



(c)

Fig. 8 Temperature vs feed with different speeds and laminate thickness of: (a) 2.6 mm, (b) 5.3 mm, and (c) 7.7 mm

shown in Fig. 8. As shown, at feed 0.025 mm/r and thickness 2.6 mm the temperature increased from 60°C to 95°C by increasing speed from 400 rpm to 1600, which means the increasing in temperature within 55%. It is also observed that, by increasing the thickness as in sequence, the temperature increases to 95°C, 112.5°C and 127.5°C, respectively at 1600 rpm and 0.025 mm/r. Increasing the thickness from 2.6 to 7.7 has a significant effect on the drill

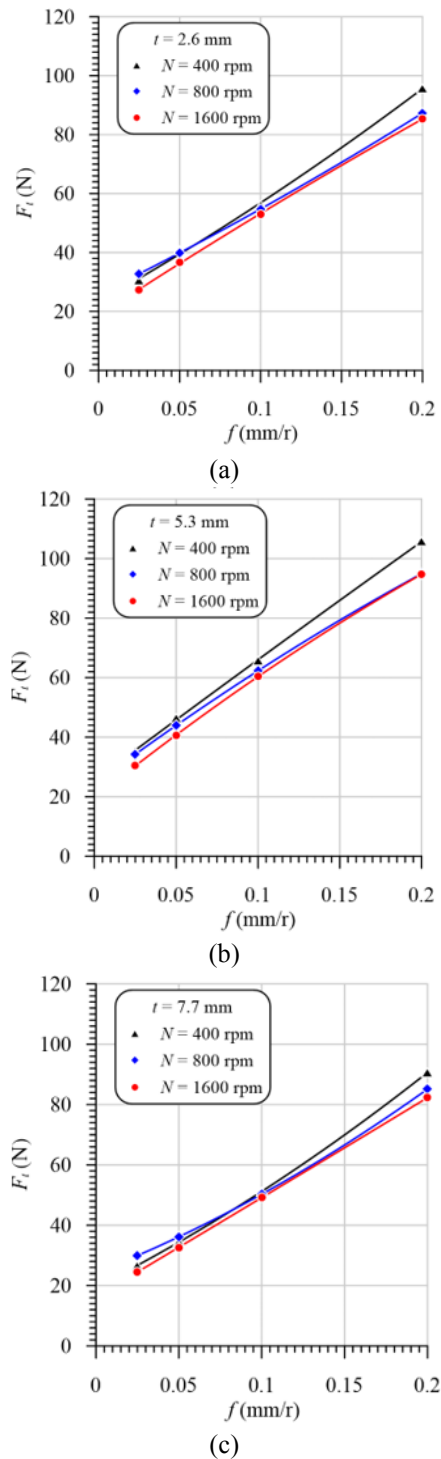


Fig. 9 Thrust force vs feed with different speeds and laminate thickness of: (a) 2.6 mm, (b) 5.3 mm, and (c) 7.7 mm

point temperature.

The increasing of the drilling temperature with cutting speed was attributed to increasing the frictional heat at the tool rake face and at the drill flanks, Ghafarizadeh *et al.* (2016). The friction between the machined surface and the drill margins as well as between chip and flutes are other reasons for increasing the measured temperature with the increase of the drill speed. It is evident from Fig. 8(c) that

the maximum drilling temperature is (128°C) obtained at maximum speed, lower feed, and maximum laminate thickness. Therefore, the drill speed and the laminate thickness are the most significant parameters on the temperature rather than feed. This conclusion is consistent with observation noticed by Zhang *et al.* (2020).

### 3.3 Effect of machining variables on thrust and torque

The effect of feed and speed on the maximum thrust force and torque in drilling GFRP laminates with thickness of 2.6, 5.3 and 7.7 mm are presented in Fig. 9. It is evident that at different laminate thicknesses, the measured thrust force decreases with a little bit as the speed increases. On comparing Fig. 8(a)-(c) with Fig. 9(a)-(c) respectively, the increase in the temperature accompanied by increasing of the drill speed leads to decreasing the thrust force in the same order of thicknesses. Xu *et al.* (2020) attributed the reduction of the thrust force with increasing drilling speed to the thermal softening of the FRP composites. Although the thinner specimens (2.6 mm) have the lowest temperature, their thrust forces are lower than those of the 5.3 mm. This behavior was attributed to the lower stiffness of the thinner specimen is more effective compared to the reduction in the stiffness of those with 5.3 mm thickness because of higher temperature and softening.

In case of smaller thickness at 2.6 mm, by increasing cutting speed from 400 rpm to 1600 rpm, the maximum thrust force is decreased by 15%. However, in the other thicknesses, this reduction is less than 15%. Through all cases spreading in Fig. 9, it is obvious that the higher the feed the higher the thrust force. So, there is a proportional significant effect of the feed on the thrust force compared to the effect of cutting speed. This result is attributed to the increasing of the cross-sectional area of the uncut chip ( $A=D.f/4$ ) with increasing feed.

It is evident from Fig. 10 that the cutting temperature was increased with increasing feed at different speeds and laminate thicknesses. This was attributed to increase of friction force between the machined surface and both drill flanks and margins and, also between chip and flutes. Increasing of the cross-sectional area of the uncut chip ( $A=D.f/4$ ) is another reason for increasing friction force on the rake face and the flank face of the tool point and thus, increasing the torque. The engaged drill body length just before the exit of chisel edge of the drill point of the laminate with 2.6 mm thickness is 0.8 mm (=2.6 mm-approach allowance, 1.8 mm) very small compared to 3.5 mm and 5.9 mm of the laminate thickness of 5.3 mm and 7.7 mm respectively. Hence, at the same cutting speeds and feeds the lowest torque is for the composite laminate with the lowest thickness (2.6 mm) because of decreasing the friction area between the drill margins and the machined hole wall surface. Also, the GFRP laminate with 2.6 mm thickness has the lower induced temperature, Fig. 8, and thus, lower thermal expansion. Increasing the drill thermal expansion can significantly increase the friction between drill margins and the machined hole wall surface. In addition, the friction between the chip and the drill flute is decreased with decreasing specimen thickness. For this reason, the torque of the GFRP laminate with 5.3 mm

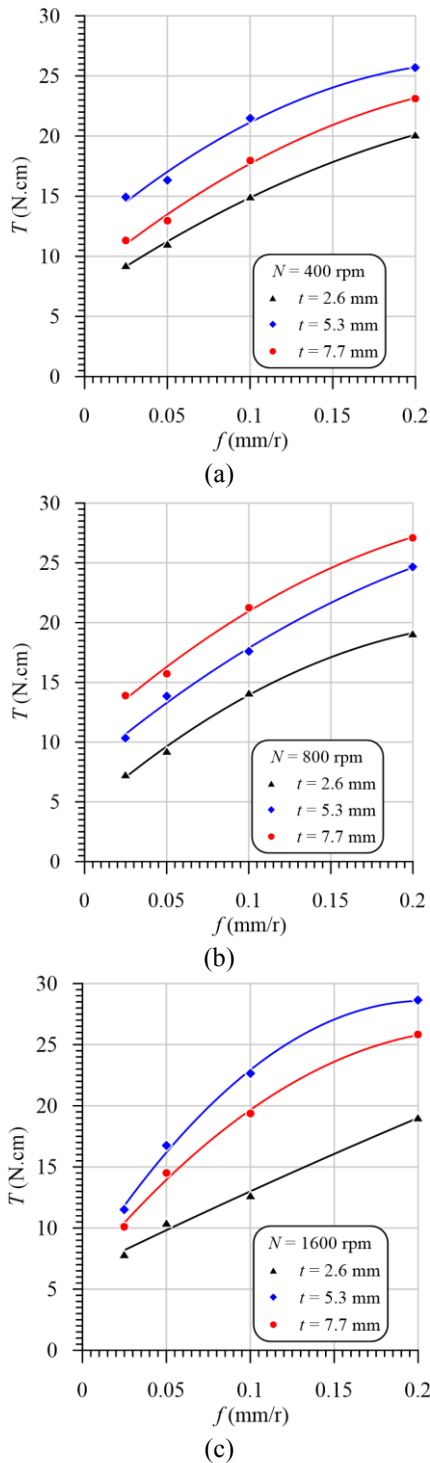


Fig. 10 Torque vs feed with different laminate thicknesses and speed of: (a) 400 rpm, (b) 800 rpm, and (c) 1600 rpm. 7.7 mm

thickness is higher than those of the 2.6 mm as shown in Fig. 10(a)-(c).

### 3.4 Effect of machining variables on the delamination factor

Delamination induced in drilling FRP composite laminates exhibited a complex failure mode that consists of

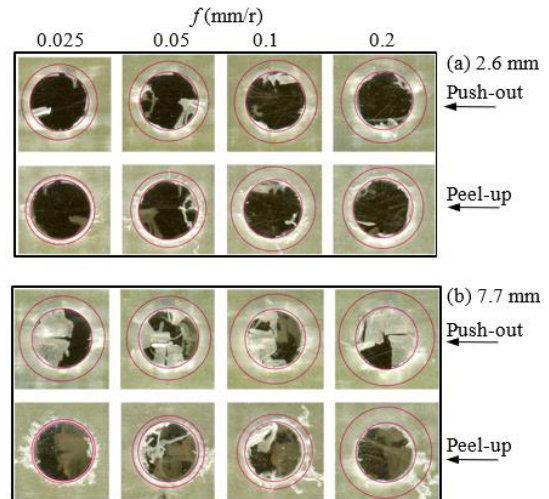


Fig. 11 Representative samples of delaminations in drilling of GFRP laminate at speed of 1600 rpm: (a)  $t=2.6$  mm and (b)  $t=7.7$  mm

a combination between mechanical and thermal damages. The delamination may occur at the entry (peel-up) and exit planes (push-out) of the composite laminate. Fig. 11 shows some representative samples of peel-up and push-out delaminations at different feeds, speeds and laminate thickness. It is evident that the push-out delamination is higher and more critical than the peel-up because of the lack of a backup support, which can compensate the thrust force during drill penetration. On comparing Fig. 11(a) with Fig. 11(b), it is evident that at the same cutting condition, the push-out delaminations of the GFRP laminate with 7.7 mm thickness evidently higher than that of 2.6 mm thickness and accompanied with edge chipping, spalling, uncut fibers. There are excessive uncut fibers spread beyond outward because fibers bend or move away from the path of the advancing tool.

Effects of feed, and laminate thickness on peel-up and push-out delamination factors in drilling GFRP composites at speeds of 400, 800 and 1600 rpm are presented in Fig 12(a)-(c) respectively. It is evident from Fig. 12 that peel-up and push-out delamination factors are increased significantly by increasing feed as a result of increasing thrust force, Fig. 9.

From Fig. 12(c), the push-out and peel-up delaminations are sharply increased with feed because of drilling at the highest speed and temperature, Fig. 9. Although the thrust force of the specimen thickness of 5.3 mm is higher than those of the 2.5 mm the push-out and peel-up delaminations of the latter one are higher than those of the former laminate. This result was attributed to the lower stiffness of the thinner laminate and thus, higher bending deflection of the last layer compared to those of 5.3 mm thickness. The delamination of the specimen with thickness of 7.7 mm is higher than those of 5.3 mm. This result was attributed to the combination between mechanical and thermal damages in drilling specimen with 7.7 mm, which has the highest cutting temperature as shown in Fig. 9. At the sever cutting conditions, higher speed (1600 rpm), feed (0.2 mm/r) the delamination of the GFRP laminate with thickness of 2.6

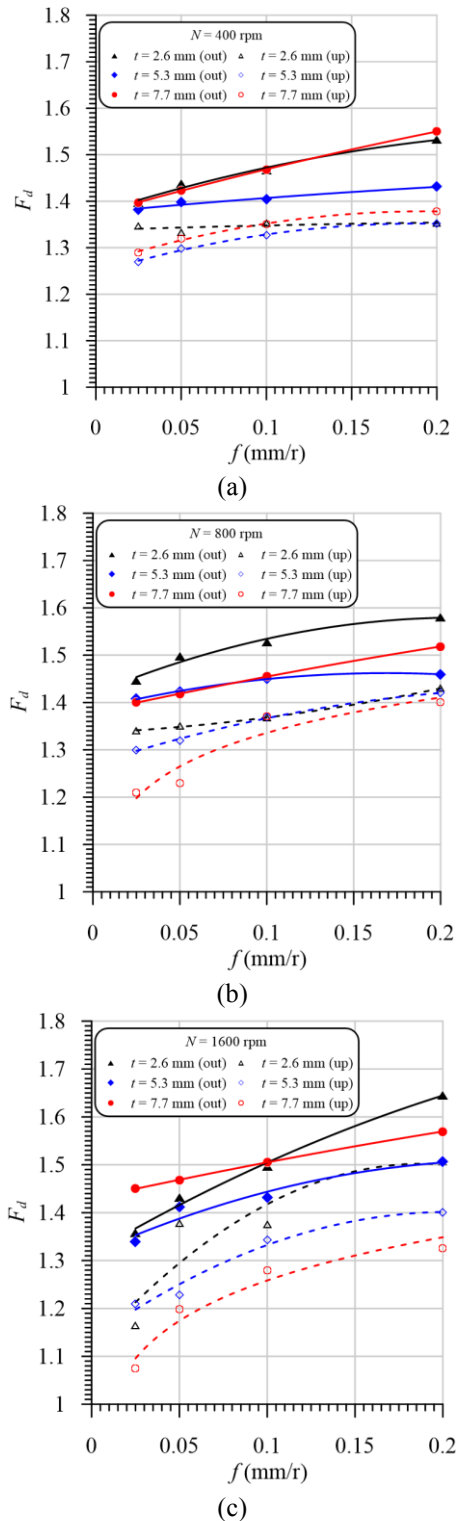


Fig. 12 Delamination factor vs feed of different laminate thickness at speed of: (a) 400 rpm, (b) 800 rpm, and (c) 1600 rpm

mm is higher than those of the 7.7 mm. This result was attributed the higher thrust force and lower stiffness of the thinner laminate. It can be concluded that feed and laminate thickness have the largest contribution to delamination damage as a result of increasing thrust forces and temperature, as shown in Fig. 9. Their study predicted that

peel-up delamination is influenced by specimen thickness and cutting speed. Whereas, push-out delamination is influenced by specimen thickness and feed.

At the beginning of drilling operation, the thickness of the laminated composite materials is able to withstand the cutting force and as the tool approaches the exit plane, the stiffness provided by the remaining plies may not be enough to bear the cutting force, causing the lamina to separate result in delamination. The delaminations that occur during drilling severely influence the mechanical characteristics of the material around the hole. To avoid these problems, it is necessary to determine the optimum conditions (feed, cutting speed and material thickness) for a particular machining operation. Therefore, the optimization technique and multivariable regression have been done in the next section to predict the optimum drilling conditions.

### 3.4 Effects of cutting time on drilling response

Fig. 13(a) to (c) is exploited to present the coupling effects between the mechanical thrust force, delamination parameter, temperature and cutting time at speed of 400 rpm, 800 rpm and 1600 rpm respectively. It is shown the thrust force and delamination has the same behaviors rather than the temperature with the variation of drilling time, which assure that the delamination is dependent proportionally on the thrust force and inversely with the temperature that may lead to the softening. Therefore, the thrust force and temperature have a coupling effect on the delamination ratio, which will be investigated statistically in the next section. From Fig. 15, it can be concluded that, by increasing the time of drilling, the temperature of drill and chip increased, and the thrust forced decreased in exponential forms.

## 4. Finite element model

### 4.1 Drill bit and workpiece modeling

The finite element model 3D solid components are the Drill bit and the workpiece. The Drill bit is modeled using a parametric generic SolidWorks model. This generic model automatically creates the 3D model of the drill body based on the drill's main geometry features; drill diameter, point angle, helix angle, clearance angle, and chisel edge size. The steps of creating the drill 3D solid body are summarized in Fig. 14. The drill model starts from a blind cylinder defined by the drill diameter and length. Four consequence cuts create the final shape of the drill. Firstly, the flute is graved by sweeping a circular profile on the helix profile (Fig. 14(a)). Second, by a wedge defined by the point angle parameter, the drill point angle is cut (Fig. 14(b)). Third, the relief angle is cut by a wedge profile parallel to the drill flank (Fig. 14(c)). Finally, the clearance cut of the drill is made by sweep cutting of a rectangular profile through the same helix profile of the flute cut (Fig. 14(d)). Finally, the drill bit's outer surface is discretized with shell elements as a rigid body, ignoring any deformation that might occurs due to its interaction with the workpiece.

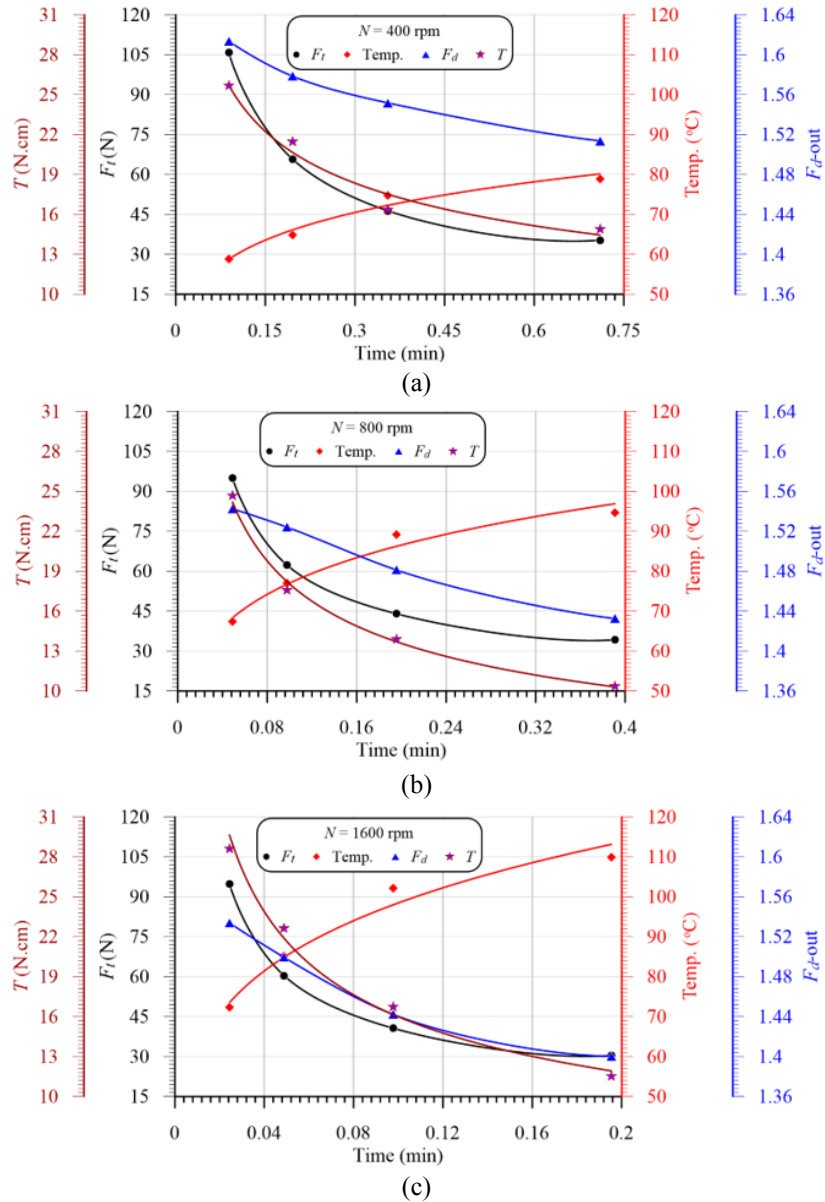


Fig. 13 Variation of thrust force, delamination, and temperature vs the cutting time at speed of: (a) 400 rpm, (b) 800 rpm, and (c) 1600 rpm

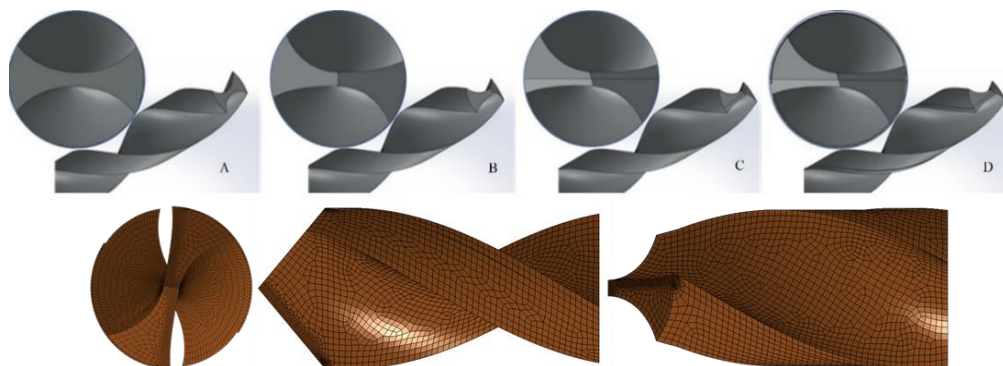


Fig. 14 Solid modeling and meshing steps of the drill bit

The finite elements of the workpiece are meant to be parallel to the drill geometry. This design is achieved by modeling the workpiece with two extra cones, as shown in

Fig. 15(a). These two cones are sliced later after creating the finite element mesh, as shown in Fig. 15(b) and Fig. 15(c). The workpiece is divided into two main parts an

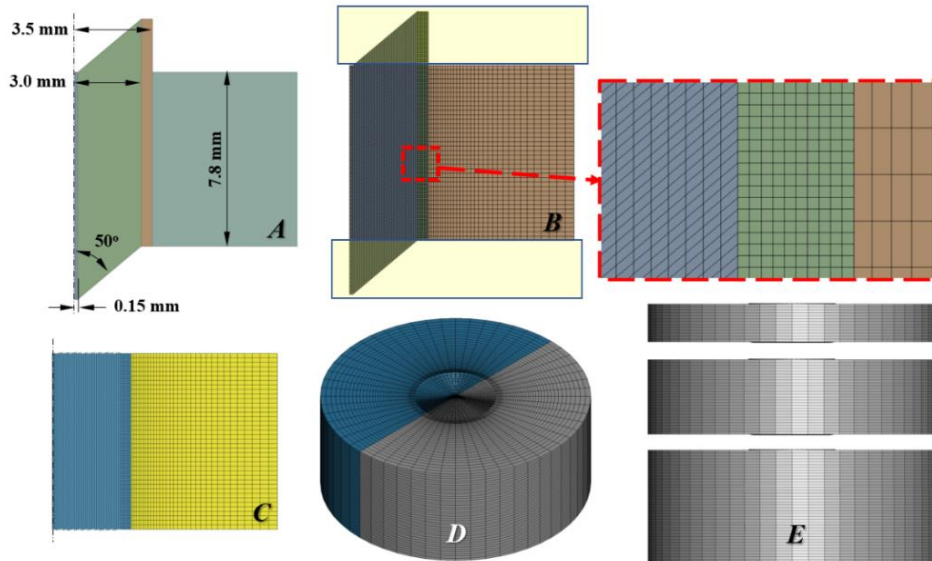


Fig. 15 Solid modeling and meshing steps of the Woven GFRP workpieces

erodible part with very fine mesh and an elastic part with coarse mesh, as shown in the zoomed figure in Fig. 15(b). The two parts are connected using a tie contact algorithm. Each of the discretized workpieces is then rotated around Z axis separately to form the workpiece's final finite element model, as shown in Fig. 15(d). The mesh size in the fine zone is 0.025 mm in the feed direction and 0.05 mm in the radial direction. In the coarse elements zone, the elements are sized at 0.1 mm in the feed direction while enlarged towards the outermost workpiece stem. The mentioned procedure is used for the workpiece with a thickness of 7.8 mm, which is eased to be cut to the other two thicknesses, 5.2 mm and 2.6 mm, without repeating the mentioned procedure, as shown in Fig. 15(e).

#### 4.2 Model setup and adaptation

The finite element model requires defining the contact between the drill and the workpiece, defining the boundary conditions and initial conditions of the drill and workpiece, defining the workpiece material properties, defining the element type, defining the erosion model, and setting the solution scheme. Due to the uncertainties in many of these model parts, a parametric study will be carried out to set up the finite element model's proper settings. The model is set at chosen settings based on the authors' experience, then based on the measured experimental results, these settings are adapted to the most accurate conditions.

The model components, drill, workpiece erodible, and elastic parts are shown in Fig. 16. The starting evaluation case is chosen with a plate thickness of 2.6 [mm], drilling feed of 0.2 [mm/rev], drill diameter of 6.0 [mm], drill point angle of 100° [deg], and fixation diameter of 20.0 [mm]. The finite element model parameters are set at starting conditions based on the authors' experience. The eroding contact's friction coefficient is assumed 0.5, and the model uses full integration solid elements (ELFORM#2) for erodible elements and constant stress solid elements (ELFORM#1) for the elastic supporting elements. The drill

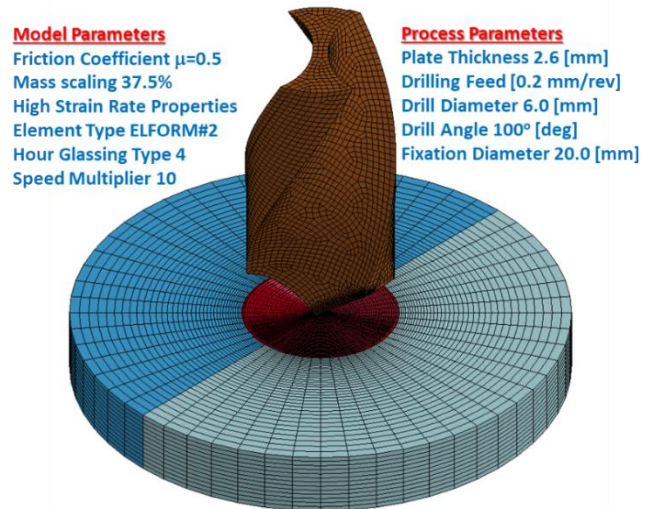


Fig. 16 Finite element model components with defined process parameters and model parameters

rotational speed is multiplied by ten for speeding up the solution, and a mass scaling factor is set at 37.5%.

The model successfully simulated the drilling of woven GFRP after about 250 hours. Fig. 17 shows the erodible elements' plastic strain contours during the drilling process's development steps while hiding the rest of the simulation model for clarity. It is worth noting that many flying chips are observed during the drilling simulation; meanwhile, no plastic strains are observed at the outermost layer of the erodible elements. The pre-chosen model parameters are then evaluated against the experimental measurements of the drilling axial thrust force and the drilling torque for the same working conditions for drilling a plate with a thickness of 2.6 [mm], drilling feed of 0.2 [mm/rev], drill diameter of 6.0 [mm], drill point angle of 100° [deg], and fixation diameter of 20.0 [mm]. The evaluated model parameters are; the model speed multiplier, the model mass scaling, the contact coefficient of friction, the material model, and the element type.

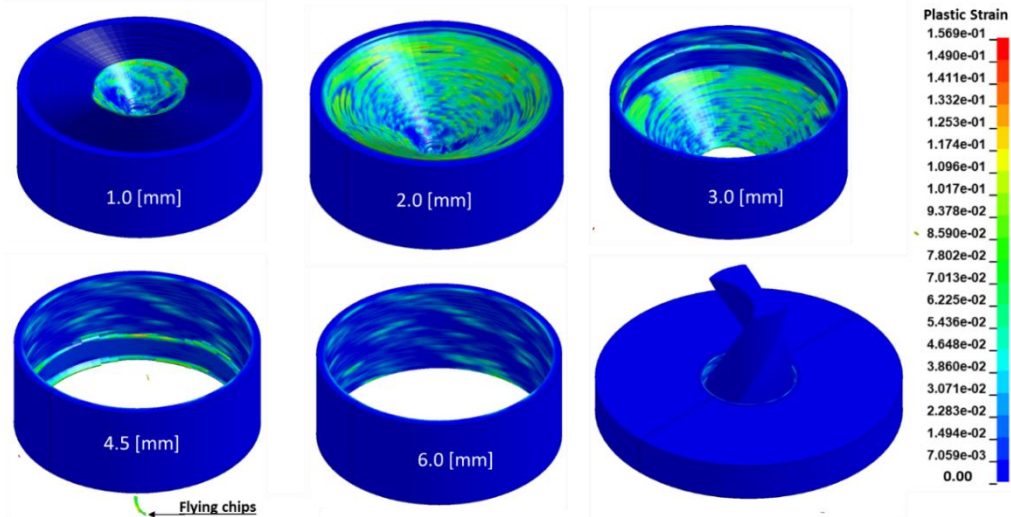


Fig. 17 Solid modeling and meshing steps of the drill bit

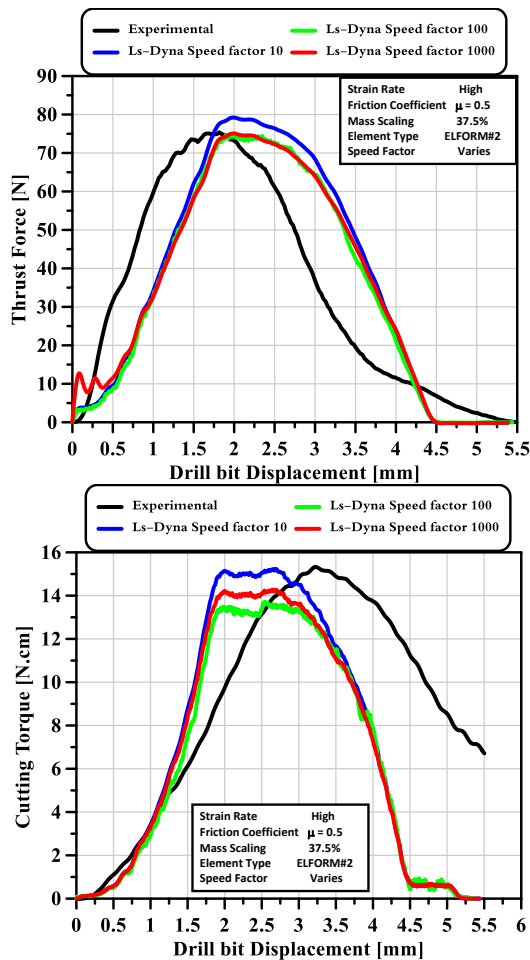


Fig. 18 Effect of the drilling speed multiplier on the drilling thrust force and torque

## 5. Numerical analysis

### 5.1 Effects of model speeding up

In the previously mentioned starting model, the drilling speed is multiplied by 10 to reduce the calculations' cost;

Table 6 Comparison of the solution times for the drilling speeding various multipliers

	Experimental	Speed Factor=1000	Speed Factor=100	Speed Factor=10
Maximum Thrust Force	75 [N]	75 [N]	74.7 [N]	79 [N]
Maximum Torque	15.3 [N.cm]	14.2 [N.cm]	13.5 [N.cm]	15.2 [N.cm]
Solution Time [min]	N/A	151 [min]	1470 [min]	14400 [min]

however, the solution time is extremely high with more than 250 hours. Since the current model neither considers the heating effects nor the strain rate effects, increasing the simulated drilling speed will not significantly change the results. The drilling speed is evaluated further at 100 times and 1000 times the real drilling speed. The other model parameters are kept the same for the three evaluation models, as shown in Fig. 18.

The comparison shows that multiplying the drilling speed with multiple orders of magnitude has slight changes in the cutting forces. However, the calculation cost is decreased dramatically to 2 hours and a half for the case of multiplying by 1000, which is one hundredth the time of the starting simulation model, as shown in Table 6. This virtual drilling speed increase helps the comprehensive exploration of woven GFRP drilling using finite element modeling, except the studies include thermal effects.

### 5.2 Effects of mass scaling

Nonphysical mass is applied to a system to obtain a greater explicit time step, defined as mass-scaling. In certain circumstances, the impact of mass scaling is negligible, and it is justifiable to incorporate nonphysical mass. In all cases, the analyst's judgment based on experimental verification determines the impact of mass scaling. In this section, three conditions are tested for mass scaling against the cutting forces and calculation cost; no mass scaling, 37.5% mass scaling, and 75% mass scaling. These evaluation cases are tested with the same process

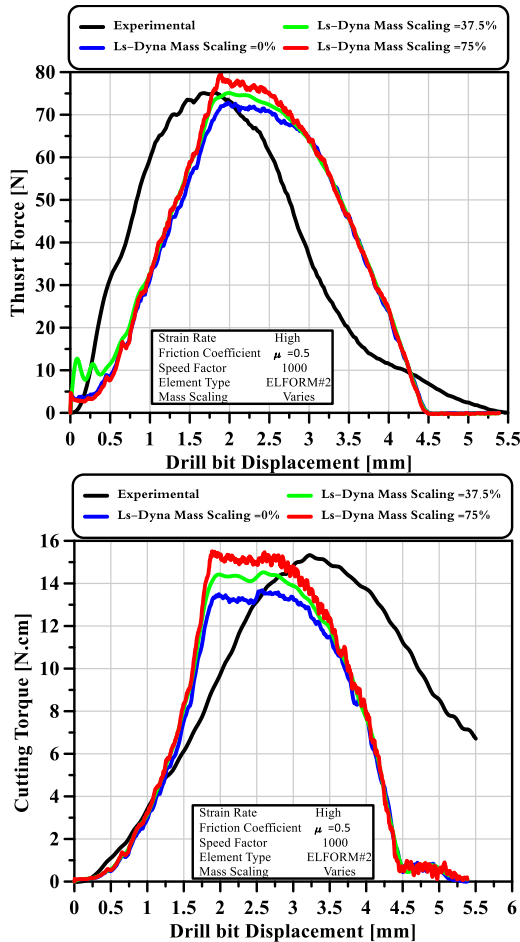


Fig. 19 Effect of the mass scaling on the drilling thrust force and torque

parameters, plate thickness 2.6 mm, drill diameter 6.0 mm, drilling feed 0.2 mm/rev, and drill point angle 118°. The finite element model's common parameters for the three evaluation cases are set at contact's friction coefficient of 0.5. The model uses full integration solid elements (ELFORM#2) for erodible elements and constant stress solid (ELFORM#1) for the elastic supporting elements. For speeding up the solution, the drill rotational speed is multiplied by one thousand. Furthermore, the material model is assumed plastic kinematic with high strain rate properties of woven glass-reinforced polymer fiber.

The finite element model results show insignificant changes in the thrust force and slight changes in the cutting torques, as shown in Fig. 19. However, the calculation time is reduced from the model with no mass scaling to the model with moderate mass scaling ten times. Further increase in the mass scaling over the recommended threshold of 40% shows insignificant calculation time savings. The further simulations stick with the moderate mass scaling of 37.5%.

### 5.3 Effects of element type

The current finite element model simulates the workpiece using 3D solid elements. Solid elements are 3D finite elements that can be used to model solid bodies and

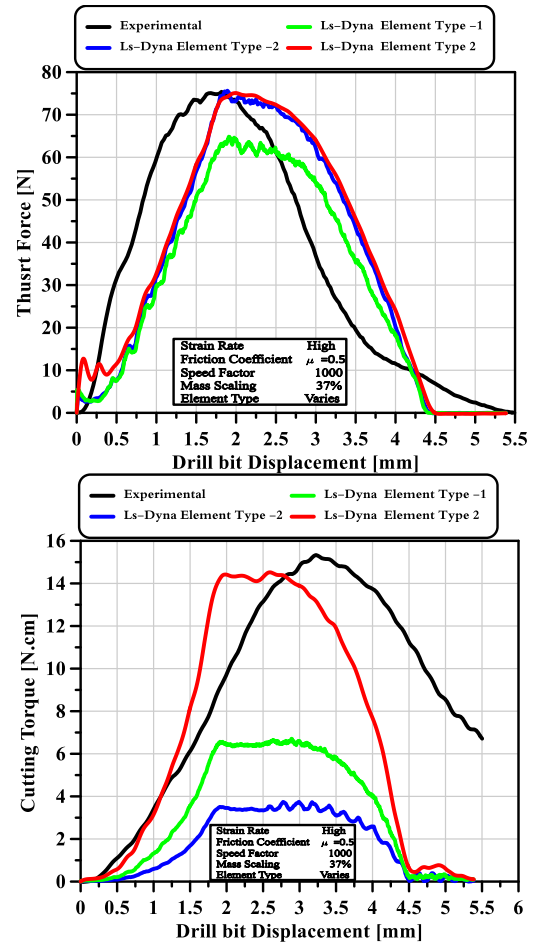


Fig. 20 Effect of the element type on the drilling thrust force and torque

structures without the requirement for any a priori geometric simplification. There are no geometric, constitutive, or loading conclusions to create the model. Further, it eases more practical treatment of boundary conditions (compared to shells or beams). Visually, the FE mesh resembles the existing system. On the other hand, brick elements sufferer expensive mesh refining, CPU time, and mesh preparation. Although hexahedral brick elements with full integration formulation require more calculation time, it is stable and accurate. Ls-Dyna offers three full integration hexahedral element types; ELFORM2, ELFORM-1, and ELFORM-2. The latter two types are more expensive than the first type, but they are used to overcome instabilities due to badly shaped elements. The three types are evaluated against the drilling thrust force and torque and the calculation time as shown in Fig. 20.

The element type evaluation results show that hexahedral brick element with full integration type 2 has accurate results with the lowest calculation time, as shown in Table 7. Element type -1 shows proper calculation time but with far inaccurate results. Element type -2 achieves close results to element type 2 but requires severely higher calculation time. Element type 2 does not suffer any instability problems that push towards the need for element type -2. The chosen element type for further simulation is element type 2.

Table 7 The effects of element type on the drilling cutting forces and the solution time

	Experimental	Element Type -1	Element Type 2	Element Type -2
Maximum Thrust Force	75 [N]	64.7 [N]	75.1 [N]	75.3 [N]
Maximum Torque	15.3 [N.cm]	12.5 [N.cm]	14.5 [N.cm]	14.0 [N.cm]
Solution Time [min]	N/A	171 [min]	151 [min]	550 [min]

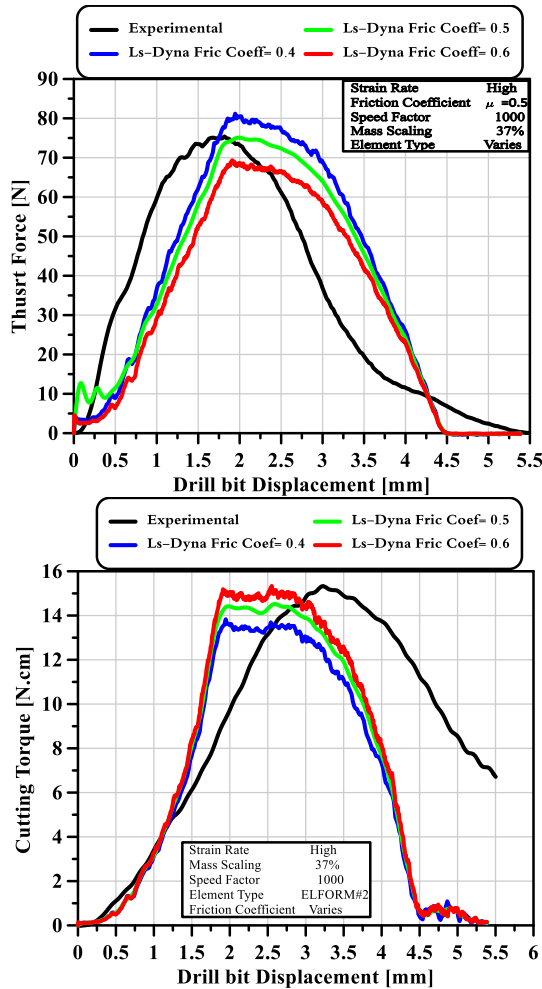


Fig. 21 Effect of the friction coefficient on the drilling thrust force and torque

5.4 Effects of coefficient of friction

Friction conditions playing a significant role in defining the cutting forces in the drilling process. The experiments are carried at dry conditions, which results in high friction conditions. These friction coefficients are not measured in the current work, requiring model adaptation for the accurate friction condition evaluation. Three friction coefficients are examined; 0.4, 0.5, and 0.6, as presented in Fig. 21. The rest of the model parameters are set at the previously chosen parameters in the previous sections. The results show that friction coefficient 0.5 is the most proper friction coefficient for the current drilling experiments on the woven glass fiber reinforced polymer.

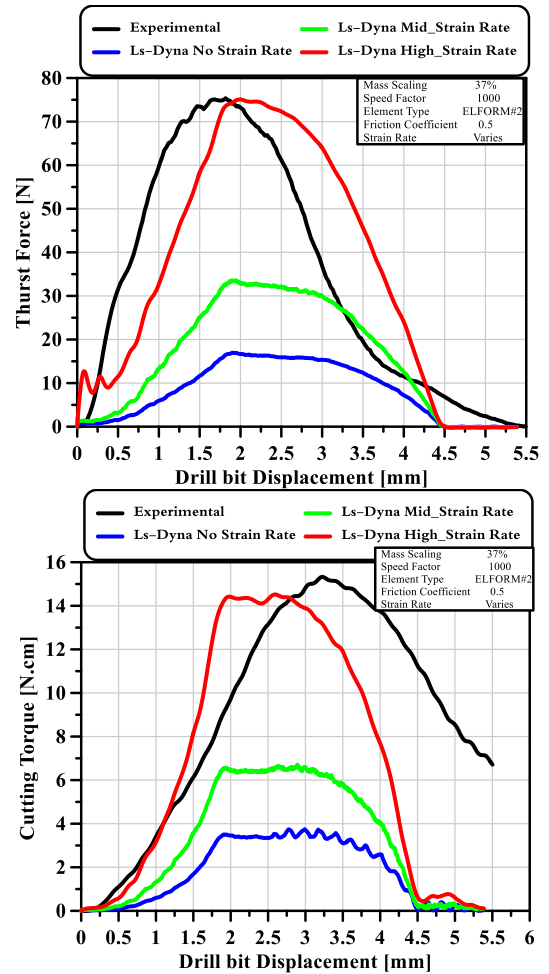


Fig. 22 Effect of Material Properties on the drilling thrust force and torque

5.5 Effects of strain rate properties

Woven glass fiber reinforced polymer behaves differently at high strain rates than at quasi-static deformation. Many researchers have measured the mechanical properties of the woven GFRP at different strain rates. These results show that the Woven GFRP is stiffer in elastic zone and stiffer after elastic zone with higher failure strain at a higher strain rate. The previous evaluation models have used the higher strain rate properties due to pre-testing models. In this section, the other strain rate conditions' effect is presented to gain confidence in the chosen finite element model parameters.

The evaluation results show a significant reduction in the drilling axial thrust and torque, as shown in Fig. 22. In drilling, the strain rate is extremely high with no change during the process. This constant high strain rate allows the use of material properties of the WGFRP at a high strain rate as the base material properties in the finite element model without strain rate effects.

6. Statistical analysis

Much research combined between DoE and ANNs to

Table 8 ANOVA results with contribution of control factors effect on machinability responses

Source	DF	$F_t$	$P$ -Value	$T$ (N.cm)	$P$ -Value	$F_{d-out}$	$P$ -Value	Temp	$P$ -Value
$f$ (mm/r)	3	95.38%	0.000	73.81%	0.000	58.50%	0.000	30.94%	0.000
$s$ (N.cm)	2	0.78%	0.040	0.12%	0.778	3.58%	0.100	34.39%	0.000
$t$ (mm)	2	3.04%	0.000	19.45%	0.000	17.86%	0.000	28.76%	0.000
Error	28	0.79%		6.61%		20.05%		5.91%	
Total	35	100.00%		100.00%		100.00%		100%	

develop prediction models Abdelwahed *et al.* (2012), El-Midany *et al.* (2013), Kharwar and Verma (2019). Yun and Abdel Wahab (2017) detected damage of composite structures using vibration data and dynamic transmissibility ensemble with an auto-associative neural network. Damage in a girder bridge was predicted using transmissibility functions as input data to Artificial Neural Networks by Nguyen *et al.* (2019). Tran-Ngoc *et al.* (2019) discovered a failure in bridges and beam-like structures by improving the training parameters of ANNs using a cuckoo search algorithm. Khatir *et al.* (2019, 2020) improved the ANNs technique combined with the Jaya algorithm for crack identification in plates using extended isogeometric analysis and experimental analysis. As outputs of drilling operation (responses), thrust force, torque, and temperature were measured during the experiment conducting. In present study, a factorial design was used to identify the main effects of three factors named feed, spindle speed, and workpiece thickness on the machinability responses mentioned above. The machining properties were measured according to design of experiments for actual independent drilling process variables with their levels illustrated in Table 5.

The primary objective for employing ANOVA was to investigate the significance of machining parameters affecting the machinability properties including thrust force, torque, cutting temperature and delamination factor. The ANOVA results are summarized in Table 6. The contribution percentage of each parameter on the total variation indicates its effect on the measured properties. The significant effect of the machining parameters on the machinability of GFRP composite can be measured by the  $P$ -value. For most experimental work, the  $P$  value less than 0.05 indicates the significance of the related factor for the response. Accordingly, all machining parameters have significant effect on the measured temperature as shown in Table 6. The largest contribution is of the speed (34.39%), followed by feed (30.94%) and thickness (28.76%).

It is evident that the contribution of the feed on measured thrust force is about 95.38%, which is higher than those of laminate thickness (3.04%). However, the effect of laminate thickness is higher than the cutting speed (0.78%), which is agreed with Figs. 9. The lower contribution of the speed was attributed to the indirect effect of increasing the temperature accompanied with decreasing stiffness of GFRP specimen on the measured force. Observing Table 6, it is evident that the torque is primarily affected by feed (73.81%) then the thickness (19.45%), while the effect of

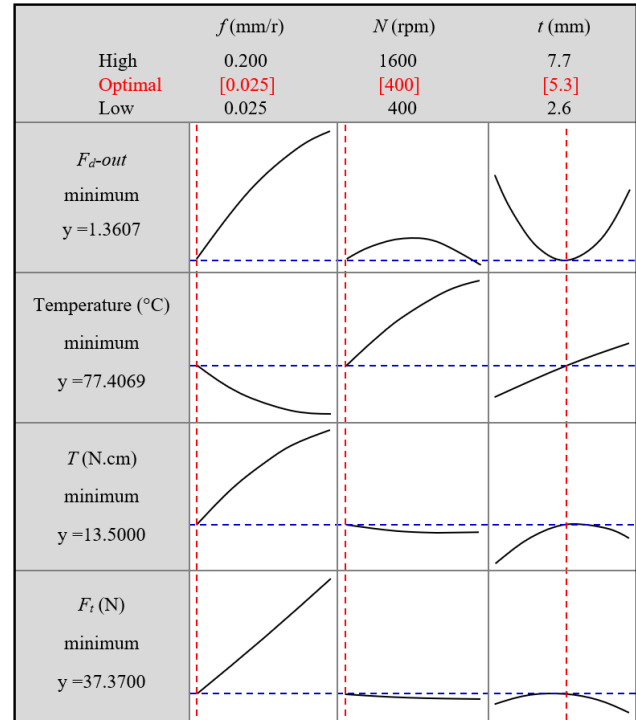


Fig. 23 Optimum response according to different machining parameters

speed is not significant ( $p=0.778$ ). The feed has the most significant drilling parameter affecting the delamination factor (58.50%) as a result of its high effect on the thrust force (95.38%). The thickness of laminate affects the delamination by 17.86%. While the spindle speed has no significant effect on delamination with  $p$ -value (0.1).

The optimization function aims to minimize all machinability properties of drilling GFRP composite. The optimization plot in Fig. 23 reveals that the optimal parameters are feed of 0.025 mm/r, speed of 400 rpm and material thickness of 5.3 mm. While, it is observed that the optimal parameters for minimum push-exit delamination, without respect to other machinability properties, are the feed of 0.025 mm/r, the speed of 1600 rpm, and the laminate thickness of 5.3 mm. This combination may produce minimum push-exit delamination but is associated with maximum temperature as shown in part of plot dedicated for temperature in Fig. 23

## 7. Conclusions

The effect of machining parameters on the thermomechanical response of the woven GFRP composite laminated under drilling process has been studied compressively through this article. The distribution of surface temperature of the heat affected zone (HAZ) and drill point temperature were investigated using thermal infrared camera and instrumented drills with thermocouples. The impact of machining parameters on the generated heat, thrust force, torque and delamination in drilling GFRP composite laminates with different thickness has been evaluated. The main outcomes from this study can

be summarized as.

- The temperature of the HAZ was sharply decreased as move away from the hole edge as a result of the lower thermal conductivity of the GFRP composite laminates.
- The increase in the temperature rises because of increasing the drill speed leads to decreasing the thrust force.
- The thrust force and temperature have a coupling effect on the delamination ratio. By increasing the cutting time, the temperature increased, and the thrust force decreased in exponential forms.
- At the same cutting condition, the push-out delaminations of the GFRP laminate with 7.7 mm thickness evidently higher than that of 2.6 mm thickness and accompanied with edge chipping, spalling, uncut fibers. This behavior was attributed to the highest temperature induced in drilling of the thicker laminate leads to softening the matrix and hence, bending the last layer instead of cutting by the drill edges.
- From ANOVA results, all drilling conditions have significant influence on generated temperature, while the feed and material thickness are seen to make the largest contribution to the delamination effect. The optimal cutting conditions are feed of 0.025 mm/r and speed of 400 rpm, when the drilling process is carried out on the GFRP laminate with 5.3 mm thickness

## Acknowledgments

This project was supported by the National Science, Technology, and Innovation Plan (NSTIP) strategic technologies program in the Kingdom of Saudi Arabia under grant number 15-ADV4307-03. The authors, gratefully appreciated to Science and Technology Unit at King Abdulaziz University for providing technical and financial support.

## References

- Abdelwahed, M.S., El-Baz, M.A. and El-Midany, T.T. (2012), "A proposed performance prediction approach for manufacturing process using ANNs", *World Acad. Sci., Eng. Technol.*, **6**, 778-783. <https://doi.org/10.5281/zenodo.1074847>.
- Ahmadi, S. and Zeinedini, A. (2020), "Experimental, theoretical and numerical investigation of the drilling effects on mode I delamination of laminated composites", *Aerosp. Sci. Technol.*, **104**, 105992. <https://doi.org/10.1016/j.ast.2020.105992>.
- Al-wandi, S., Ding, S. and Mo, J. (2017), "An approach to evaluate delamination factor when drilling carbon fiber-reinforced plastics using different drill geometries: experiment and finite element study", *Int. J. Adv. Manuf. Technol.*, **93**(9-12), 4043-4061. <https://doi.org/10.1007/s00170-017-0880-2>.
- Almitani, K.H., Abdelrahman, A.A. and Eltaher, M.A. (2020), "Stability of perforated nanobeams incorporating surface energy effects", *Steel Compos. Struct.*, **35**(4), 555-566. <https://doi.org/10.12989/scs.2020.35.4.555>.
- Almitani, K.H., Eltaher, M.A., Abdelrahman, A.A. and Abd-El-Mottaleb, H.E. (2021), "Finite element based stress and vibration analysis of axially functionally graded rotating beams", *Struct. Eng. Mech.*, **79**(1), 23-33. <https://doi.org/10.12989/sem.2021.79.1.023>.
- Asiri, S.A., Akbas, S.D. and Eltaher, M.A. (2020), "Damped dynamic responses of a layered functionally graded thick beam under a pulse load", *Struct. Eng. Mech.*, **75**(6), 713-722. <https://doi.org/10.12989/sem.2020.75.6.713>.
- Beylergil, B., Tanoglu, M. and Aktas, E. (2019), "Mode-I fracture toughness of carbon fiber/epoxy composites interleaved by aramid nonwoven veils", *Steel Compos. Struct.*, **31**(2), 113-123. <https://doi.org/10.12989/scs.2019.31.2.113>.
- Bhat, R., Mohan, N., Sharma, S., Pai, D. and Kulkarni, S. (2020), "Multiple response optimisation of process parameters during drilling of GFRP composite with a solid carbide twist drill", *Mater. Today: Proc.*, **28**, 2039-2046. <https://doi.org/10.1016/j.matpr.2020.02.384>.
- Biswal, M., Sahu, S.K., Asha, A.V. and Nanda, N. (2016), "Hygrothermal effects on buckling of composite shell experimental and FEM results", *Steel Compos. Struct.*, **22**(6), 1445-1463. <https://doi.org/10.12989/scs.2016.22.6.1445>.
- Cadorin, N., Zitoune, R., Seitier, P. and Collombet, F. (2015), "Analysis of damage mechanism and tool wear while drilling of 3D woven composite materials using internal and external cutting fluid", *J. Compos. Mater.*, **49**(22), 2687-2703. <https://doi.org/10.1177/0021998314553045>.
- Chandrasekharan, V., Kapoor, S.G. and DeVor, R.E. (1995), "A mechanistic approach to predicting the cutting forces in drilling: with application to fiber-reinforced composite materials", *J. Eng. Indus.*, **117**(4), 559-570. <https://doi.org/10.1115/1.2803534>.
- Di Benedetto, R.M., Botelho, E.C., Janotti, A., Junior, A.A. and Gomes, G.F. (2021), "Development of an artificial neural network for predicting energy absorption capability of thermoplastic commingled composites", *Compos. Struct.*, 113131. <https://doi.org/10.1016/j.compstruct.2020.113131>.
- Durão, L.M.P., Gonçalves, D.J., Tavares, J.M.R., de Albuquerque, V.H.C., Vieira, A.A. and Marques, A.T. (2010), "Drilling tool geometry evaluation for reinforced composite laminates", *Compos. Struct.*, **92**(7), 1545-1550. <https://doi.org/10.1016/j.compstruct.2009.10.035>.
- El-Midany, T.T., El-Baz, M.A. and Abd-ElWahed, M.S. (2020), "A proposed performance prediction approach for manufacturing process using Artificial Neural Networks (Dept. M)", *MEJ. Mansoura Eng. J.*, **36**(4), 39-49. <https://doi.org/10.21608/bfemu.2020.122176>.
- El-Midany, T.T., El-Baz, M.A. and Abdelwahed, M.S. (2013), "Improve characteristics of manufactured products using artificial neural network performance prediction model", *Int. J. Rec. Adv. Mech. Eng.*, **2**(4), 23-34.
- Elamary, A.S. and Abd-Elwahab, R.K. (2016), "Numerical simulation of concrete beams reinforced with composite GFRP-Steel bars under three points bending", *Struct. Eng. Mech.*, **57**(5), 937-949. <https://doi.org/10.12989/sem.2016.57.5.937>.
- Eltaher, M.A. and Abdelrahman, A.A. (2020), "Bending behavior of squared cutout nanobeams incorporating surface stress effects", *Steel Compos. Struct.*, **36**(2), 143-161. <http://doi.org/10.12989/scs.2020.36.2.143>.
- Eltaher, M.A. and Akbas, S.D. (2020), "Transient response of 2D functionally graded beam structure", *Struct. Eng. Mech.*, **75**(3), 357-367. <https://doi.org/10.12989/sem.2020.75.3.357>.
- Eltaher, M.A. and Mohamed, S.A. (2020), "Buckling and stability analysis of sandwich beams subjected to varying axial loads", *Steel Compos. Struct.*, **34**(2), 241-260. <https://doi.org/10.12989/scs.2020.34.2.241>.
- Fazilati, J. (2018), "Stability of tow-steered curved panels with geometrical defects using higher order FSM", *Steel Compos. Struct.*, **28**(1), 25-37. <https://doi.org/10.12989/scs.2018.28.1.025>.
- Feito, N., Muñoz-Sánchez, A., Díaz-Álvarez, A. and Miguelez, M.H. (2019), "Multi-objective optimization analysis of cutting parameters when drilling composite materials with special geometry drills", *Compos. Struct.*, **225**, 111187. <https://doi.org/10.1016/j.compstruct.2019.111187>.

- Formisano, A., Papa, I., Lopresto, V. and Langella, A. (2019), "Influence of the manufacturing technology on impact and flexural properties of GF/PP commingled twill fabric laminates", *J. Mater. Proc. Technol.*, **274**, 116275. <https://doi.org/10.1016/j.jmatprotec.2019.116275>.
- Gaitonde, V.N., Karnik, S.R., Rubio, J.C., Correia, A.E., Abrao, A.M. and Davim, J.P. (2011), "A study aimed at minimizing delamination during drilling of CFRP composites", *J. Compos. Mater.*, **45**(22), 2359-2368. <https://doi.org/10.1177/0021998311401087>.
- Geier, N., Davim, J.P. and Szalay, T. (2019), "Advanced cutting tools and technologies for drilling carbon fibre reinforced polymer (CFRP) composites: a review", *Compos. Part A: Appl. Sci. Manuf.*, **125**, 105552. <https://doi.org/10.1016/j.compositesa.2019.105552>.
- Gemi, L., Köklü, U., Yazman, Ş. and Morkavuk, S. (2020a), "The effects of stacking sequence on drilling machinability of filament wound hybrid composite pipes: Part-1 mechanical characterization and drilling tests", *Compos. Part B: Eng.*, **186**, 107787. <https://doi.org/10.1016/j.compositesb.2020.107787>.
- Gemi, L., Morkavuk, S., Köklü, U. and Yazman, Ş. (2020b), "The effects of stacking sequence on drilling machinability of filament wound hybrid composite pipes: Part-2 damage analysis and surface quality", *Compos. Struct.*, **235**, 111737. <https://doi.org/10.1016/j.compstruct.2019.111737>.
- Geng, D., Liu, Y., Shao, Z., Lu, Z., Cai, J., Li, X., ... & Zhang, D. (2019), "Delamination formation, evaluation and suppression during drilling of composite laminates: a review", *Compos. Struct.*, **216**, 168-186. <https://doi.org/10.1016/j.compstruct.2019.02.099>.
- Ghafari-zadeh, S., Lebrun, G. and Chatelain, J.F. (2016), "Experimental investigation of the cutting temperature and surface quality during milling of unidirectional carbon fiber reinforced plastic", *J. Compos. Mater.*, **50**(8), 1059-1071. <https://doi.org/10.1177/0021998315587131>.
- Ghosh, A. and Chakravorty, D. (2019), "Application of FEM on first ply failure of composite hyper shells with various edge conditions", *Steel Compos. Struct.*, **32**(4), 423-441. <https://doi.org/10.12989/scs.2019.32.4.423>.
- Guenfoud, H., Himeur, M., Ziou, H. and Guenfoud, M. (2018), "The use of the strain approach to develop a new consistent triangular thin flat shell finite element with drilling rotation", *Struct. Eng. Mech.*, **68**(4), 385-398. <http://doi.org/10.12989/sem.2018.68.4.385>.
- Heidary, H., Mehrpouya, M.A., Saghafi, H. and Minak, G. (2020), "Critical thrust force and feed rate determination in drilling of GFRP laminate with backup plate", *Struct. Eng. Mech.*, **73**(6), 631-640. <http://doi.org/10.12989/sem.2020.723.6.631>.
- Ho-Cheng, H. and Dharan, C.K.H. (1990), "Delamination during drilling in composite laminates", *J. Eng. Indus.*, **112**(3), 236-239. <https://doi.org/10.1115/1.2899580>.
- Hou, G., Zhang, K., Fan, X., Luo, B., Cheng, H., Yan, X. and Li, Y. (2020), "Analysis of exit-ply temperature characteristics and their effects on occurrence of exit-ply damages during UD CFRP drilling", *Compos. Struct.*, **231**, 111456. <https://doi.org/10.1016/j.compstruct.2019.111456>.
- Hrechuk, A., Bushlya, V. and Ståhl, J.E. (2018), "Hole-quality evaluation in drilling fiber-reinforced composites", *Compos. Struct.*, **204**, 378-387. <https://doi.org/10.1016/j.compstruct.2018.07.105>.
- Ismail, S.O., Ojo, S.O. and Dhakal, H.N. (2017), "Thermo-mechanical modelling of FRP cross-ply composite laminates drilling: Delamination damage analysis", *Compos. Part B: Eng.*, **108**, 45-52. <https://doi.org/10.1016/j.compositesb.2016.09.100>.
- Jia, Z., Chen, C., Wang, F. and Zhang, C. (2020b), "Analytical study of delamination damage and delamination-free drilling method of CFRP composite", *J. Mater. Proc. Technol.*, **282**, 116665. <https://doi.org/10.1016/j.jmatprotec.2020.116665>.
- Jia, Z.Y., Zhang, C., Wang, F.J., Fu, R. and Chen, C. (2020a), "Multi-margin drill structure for improving hole quality and dimensional consistency in drilling Ti/CFRP stacks", *J. Mater. Proc. Technol.*, **276**, 116405. <https://doi.org/10.1016/j.jmatprotec.2019.116405>.
- Joshi, H.S., Pal, S.K. and Chakraborty, G. (2018), "Study on the delamination of GFRP composites in drilling: A finite element model", *Simulations for Design and Manufacturing*, Springer, Singapore.
- Karimi, N.Z., Heidary, H. and Minak, G. (2016), "Critical thrust and feed prediction models in drilling of composite laminates", *Compos. Struct.*, **148**, 19-26. <http://doi.org/10.1016/j.compstruct.2016.03.059>.
- Kharazan, M., Sadr, M.H. and Kiani, M. (2014), "Delamination growth analysis in composite laminates subjected to low velocity impact", *Steel Compos. Struct.*, **17**(4), 387-403. <https://doi.org/10.12989/scs.2014.17.4.387>.
- Kharwar, P.K. and Verma, R.K. (2019), "Grey embedded in artificial neural network (ANN) based on hybrid optimization approach in machining of GFRP epoxy composites", *FME Trans.*, **47**(3), 641-648. <https://doi.org/10.5937/fmet1903641P>.
- Khshaba, U.A. (2013), "Drilling of polymer matrix composites: a review", *J. Compos. Mater.*, **47**(15), 1817-1832. <https://doi.org/10.1177/0021998312451609>.
- Khshaba, U.A. and El-Keran, A.A. (2017), "Drilling analysis of thin woven glass-fiber reinforced epoxy composites", *J. Mater. Proc. Technol.*, **249**, 415-425. <http://doi.org/10.1016/j.jmatprotec.2017.06.011>.
- Khshaba, U.A. and Othman, R. (2017), "Low-velocity impact of woven CFRE composites under different temperature levels", *Int. J. Impact Eng.*, **108**, 191-204. <http://doi.org/10.1016/j.ijimpeng.2017.04.023>.
- Khshaba, U.A., Abd-Elwahed, M.S., Ahmed, K.I., Najjar, I., Melaibari, A. and Eltaher, M.A. (2020), "Analysis of the machinability of GFRE composites in drilling processes", *Steel Compos. Struct.*, **36**(4), 417-426. <https://doi.org/10.12989/scs.2020.36.4.417>.
- Khshaba, U.A., El-Sonbaty, I.A., Selmy, A.I. and Megahed, A.A. (2010a), "Machinability analysis in drilling woven GFR/epoxy composites: Part I-Effect of machining parameters", *Compos. Part A: Appl. Sci. Manuf.*, **41**(3), 391-400. <https://doi.org/10.1016/j.compositesa.2009.11.006>.
- Khshaba, U.A., El-Sonbaty, I.A., Selmy, A.I. and Megahed, A.A. (2010b), "Machinability analysis in drilling woven GFR/epoxy composites: Part II-Effect of drill wear", *Compos. Part A: Appl. Sci. Manuf.*, **41**(9), 1130-1137. <https://doi.org/10.1016/j.compositesa.2010.04.011>.
- Khshaba, U.A., Seif, M.A. and Elhamid, M.A. (2007), "Drilling analysis of chopped composites", *Compos. Part A: Appl. Sci. Manuf.*, **38**(1), 61-70. <https://doi.org/10.1016/j.compositesa.2006.01.020>.
- Kumar, J., Verma, R.K. and Debnath, K. (2020), "A new approach to control the delamination and thrust force during drilling of polymer nanocomposites reinforced by graphene oxide/carbon fiber", *Compos. Struct.*, **253**, 112786. <https://doi.org/10.1016/j.compstruct.2020.112786>.
- Liu, S., Yang, T., Liu, C., Jin, Y., Sun, D. and Shen, Y. (2020a), "An analytical delamination model of drilling aramid fiber-reinforced plastics by brad drill", *Int. J. Adv. Manuf. Technol.*, **108**(9), 3279-3290. <https://doi.org/10.1007/s00170-020-05628-9>.
- Liu, S., Yang, T., Liu, C., Jin, Y., Sun, D. and Shen, Y. (2020b), "Modelling and experimental validation on drilling delamination of aramid fiber reinforced plastic composites", *Compos. Struct.*, **236**, 111907. <https://doi.org/10.1016/j.compstruct.2020.111907>.
- Lu, L., She, G.L. and Guo, X. (2021), "Size-dependent

- postbuckling analysis of graphene reinforced composite microtubes with geometrical imperfection”, *Int. J. Mech. Sci.*, **199**, 106428. <https://doi.org/10.1016/j.ijmecsci.2021.106428>.
- Luo, B., Li, Y., Zhang, K., Cheng, H. and Liu, S. (2016), “Effect of workpiece stiffness on thrust force and delamination in drilling thin composite laminates”, *J. Compos. Mater.*, **50**(5), 617-625. <https://doi.org/10.1177/0021998315580449>.
- Mahieddine, A., Ouali, M. and Mazouz, A. (2015), “Modeling and simulation of partially delaminated composite beams”, *Steel Compos. Struct.*, **18**(5), 1119-1127. <https://doi.org/10.12989/scs.2015.18.5.1119>.
- Merino-Pérez, J.L., Royer, R., Ayvar-Soberanis, S., Merson, E. and Hodzic, A. (2015), “On the temperatures developed in CFRP drilling using uncoated WC-Co tools Part I: Workpiece constituents, cutting speed and heat dissipation”, *Compos. Struct.*, **123**, 161-168. <https://doi.org/10.1016/j.compstruct.2014.12.033>.
- Merino-Pérez, J.L., Royer, R., Merson, E., Lockwood, A., Ayvar-Soberanis, S. and Marshall, M.B. (2016), “Influence of workpiece constituents and cutting speed on the cutting forces developed in the conventional drilling of CFRP composites”, *Compos. Struct.*, **140**, 621-629. <https://doi.org/10.1016/j.compstruct.2016.01.008>.
- Mishra, P.K., Pradhan, A.K., Pandit, M.K. and Panda, S.K. (2020), “Thermoelastic effect on inter-laminar embedded delamination characteristics in Spar Wingskin Joints made with laminated FRP composites”, *Steel Compos. Struct.*, **35**(3), 439. <https://doi.org/10.12989/scs.2020.35.3.439>.
- Mudhukrishnan, M., Hariharan, P. and Palanikumar, K. (2020), “Measurement and analysis of thrust force and delamination in drilling glass fiber reinforced polypropylene composites using different drills”, *Measure.*, **149**, 106973. <https://doi.org/10.1016/j.measurement.2019.106973>.
- Murthy, B.R.N., GS, V., Narayan, S., Naik, N., Sooriyaperakasm, N., Karthik, A. and Borkhade, R. (2019), “Mechanical modelling and simulation of thrust force in drilling process in GFRP composite laminates: A novel system dynamics approach”, *Cogent Eng.*, **6**(1), 1706981. <https://doi.org/10.1080/23311916.2019.1706981>.
- Narasimhan, K. (2004), *The Six Sigma Handbook Revised and Expanded: A Complete Guide for Greenbelts, Blackbelts, and Managers at All Levels*, The TQM Magazine.
- Ojo, S.O., Ismail, S.O., Paggi, M. and Dhakal, H.N. (2017), “A new analytical critical thrust force model for delamination analysis of laminated composites during drilling operation”, *Compos. Part B: Eng.*, **124**, 207-217. <https://doi.org/10.1016/j.compositesb.2017.05.039>.
- Qiu, X., Li, P., Li, C., Niu, Q., Chen, A., Ouyang, P. and Ko, T. J. (2018), “Study on chisel edge drilling behavior and step drill structure on delamination in drilling CFRP”, *Compos. Struct.*, **203**, 404-413. <https://doi.org/10.1016/j.compstruct.2018.07.007>.
- Ramesh, B., Elayaperumal, A., Satishkumar, S., Kumar, A., Jayakumar, T. and Dinakaran, D. (2016), “Influence of cooling on the performance of the drilling process of glass fibre reinforced epoxy composites”, *Arch. Civil Mech. Eng.*, **16**, 135-146. <http://doi.org/10.1016/j.acme.2015.03.001>.
- Reisgen, U., Schiebahn, A., Lotte, J., Hopmann, C., Schneider, D. and Neuhaus, J. (2020), “Innovative joining technology for the production of hybrid components from FRP and metals”, *J. Mater. Proc. Technol.*, **282**, 116674. <https://doi.org/10.1016/j.jmatprotec.2020.116674>.
- Saoudi, J., Zitoun, R., Mezlini, S., Gururaja, S. and Seitier, P. (2016), “Critical thrust force predictions during drilling: analytical modeling and X-ray tomography quantification”, *Compos. Struct.*, **153**, 886-894. <https://doi.org/10.1016/j.compstruct.2016.07.015>.
- Shahri, M.N., Najafabadi, M.A. and Akhlaghi, M. (2020), “On the improvement of analytical delamination model for drilling of laminated composites using Galerkin method”, *Compos. Part B: Eng.*, **194**, 108021. <https://doi.org/10.1016/j.compositesb.2020.108021>.
- She, G.L. (2020), “Wave propagation of FG polymer composite nanoplates reinforced with GNPs”, *Steel Compos. Struct.*, **37**(1), 27-35. <https://doi.org/10.12989/scs.2020.37.1.027>.
- She, G.L. (2021), “Guided wave propagation of porous functionally graded plates: The Effect of thermal loadings”, *J. Therm. Stress.*, **44**(10), 1289-1305. <https://doi.org/10.1080/01495739.2021.1974323>.
- She, G.L., Liu, H.B. and Karami, B. (2021), “Resonance analysis of composite curved microbeams reinforced with graphene nanoplatelets”, *Thin Wall. Struct.*, **160**, 107407. <https://doi.org/10.1016/j.tws.2020.107407>.
- Shetty, N., Shahabaz, S.M., Sharma, S.S. and Shetty, S.D. (2017), “A review on finite element method for machining of composite materials”, *Compos. Struct.*, **176**, 790-802. <https://doi.org/10.1016/j.compstruct.2017.06.012>.
- Shyha, I.S., Aspinwall, D.K., Soo, S.L. and Bradley, S. (2009), “Drill geometry and operating effects when cutting small diameter holes in CFRP”, *Int. J. Mach. Tool. Manuf.*, **49**(12-13), 1008-1014. <https://doi.org/10.1016/j.ijmachtools.2009.05.009>.
- Suresh, M., Sanders, A., Prajapati, P., Kaipa, K. and Kravchenko, O.G. (2020), “Composite sandwich repair using through-thickness reinforcement with robotic hand micro-drilling”, *Compos. Struct.*, **248**, 112473. <https://doi.org/10.1016/j.compstruct.2020.112473>.
- Tagliaferri, V., Caprino, G. and Diterlizzi, A. (1990), “Effect of drilling parameters on the finish and mechanical properties of GFRP composites”, *Int. J. Mach. Tool. Manuf.*, **30**(1), 77-84. [https://doi.org/10.1016/0890-6955\(90\)90043-1](https://doi.org/10.1016/0890-6955(90)90043-1).
- Tan, C.L. and Azmi, A.I. (2017), “Analytical study of critical thrust force for on-set delamination damage of drilling hybrid carbon/glass composite”, *Int. J. Adv. Manuf. Technol.*, **92**(1-4), 929-941. <https://doi.org/10.1007/s00170-017-0152-1>.
- Tang, W., Chen, Y., Yang, H., Wang, H. and Yao, Q. (2018), “Numerical investigation of delamination in drilling of carbon fiber reinforced polymer composites”, *Appl. Compos. Mater.*, **25**(6), 1419-1439. <https://doi.org/10.1007/s10443-018-9675-3>.
- Tian, T. and Cole, K.D. (2012), “Anisotropic thermal conductivity measurement of carbon-fiber/epoxy composite materials”, *Int. J. Heat Mass Transf.*, **55**(23-24), 6530-6537. <https://doi.org/10.1016/j.ijheatmasstransfer.2012.06.059>.
- Tong, Z., Chen, Y., Huang, Q., Song, X., Luo, B. and Xu, X. (2020), “Experimental and analytical study on continuous GFRP-concrete decks with steel bars”, *Struct. Eng. Mech.*, **76**(6), 737-749. <https://doi.org/10.12989/sem.2020.76.6.737>.
- Wang, Q. and Jia, X. (2020), “Multi-objective optimization of CFRP drilling parameters with a hybrid method integrating the ANN, NSGA-II and fuzzy C-means”, *Compos. Struct.*, **235**, 111803. <https://doi.org/10.1016/j.compstruct.2019.111803>.
- Zhang, B., Wang, F., Wang, Q. and Zhao, X. (2021), “Novel fiber fracture criteria for revealing forming mechanisms of burrs and cracking at hole-exit in drilling Carbon Fiber Reinforced Plastic”, *J. Mater. Proc. Technol.*, **289**, 116934. <https://doi.org/10.1016/j.jmatprotec.2020.116934>.
- Zhang, B., Wang, F., Wang, X., Li, Y. and Wang, Q. (2020), “Optimized selection of process parameters based on reasonable control of axial force and hole-exit temperature in drilling of CFRP”, *Int. J. Adv. Manuf. Technol.*, **110**(3), 797-812. <https://doi.org/10.1007/s00170-020-05868-9>.
- Zhang, Y.Y., Wang, X.Y., Zhang, X., Shen, H.M., and She, G.L. (2021), “On snap-buckling of FGCNT reinforced nanobeams considering surface effects”, *Steel Compos. Struct.*, **8**(3), 293-304. <https://doi.org/10.12989/scs.2021.38.3.293>.
- Zitoun R, Cadorn N, Collombet F, Sima M. (2017),

“Temperature and wear analysis in function of the cutting tool coating when drilling of composite structure: In situ measurement by optical fiber”, *Wear*, **377**(15), 1849-1858. <https://doi.org/10.1016/j.wear.2016.12.015>.

Zou, F., Dang, J., Cai, X., An, Q., Ming, W. and Chen, M. (2020), “Hole quality and tool wear when dry drilling of a new developed metal/composite co-cured material”, *Proc. Inst. Mech. Eng., Part B: J. Eng. Manuf.*, **234**(6-7), 980-992. <https://doi.org/10.1177/0954405420901420> .

CC